Title

Serotonergic neurons translate taste detection into internal nutrient regulation

Journal

Neuron, 110(6)

ISSN

0896-6273

Authors

Yao, Zepeng

Scott, Kristin

Publication Date

2022-03-01

DOI

10.1016/j.neuron.2021.12.028

Peer reviewed

Published in final edited form as:

Neuron. 2022 March 16; 110(6): 1036–1050.e7. doi:10.1016/j.neuron.2021.12.028.

Serotonergic neurons translate taste detection into internal nutrient regulation

Zepeng Yao[1,*], **Kristin Scott**[1,2,3,*]

[1]Department of Molecular and Cell Biology, University of California, Berkeley, Berkeley, CA 94720, USA

[2]Helen Wills Neuroscience Institute, University of California, Berkeley, Berkeley, CA 94720, USA

[3]Lead contact

SUMMARY

The nervous and endocrine systems coordinately monitor and regulate nutrient availability to maintain energy homeostasis. Sensory detection of food regulates internal nutrient availability in a manner that anticipates food intake, but sensory pathways that promote anticipatory physiological changes remain unclear. Here, we identify serotonergic (5-HT) neurons as critical mediators that transform gustatory detection by sensory neurons into the activation of insulin-producing cells and enteric neurons in *Drosophila*. One class of 5-HT neurons responds to gustatory detection of sugars, excites insulin-producing cells, and limits consumption, suggesting that they anticipate increased nutrient levels and prevent overconsumption. A second class of 5-HT neurons responds to gustatory detection of bitter compounds and activates enteric neurons to promote gastric motility, likely to stimulate digestion and increase circulating nutrients upon food rejection. These studies demonstrate that 5-HT neurons relay acute gustatory detection to divergent pathways for longer-term stabilization of circulating nutrients.

In brief

Yao and Scott discover two distinct classes of serotonergic (5-HT) neurons in *Drosophila* that respond to taste detection and preemptively regulate feeding and endocrine and digestive function. This work provides insight into the diverse functions of 5-HT sub-circuits and the neural basis for anticipatory regulation of nutrient homeostasis.

Graphical Abstract

[*]Correspondence: zepengyao@berkeley.edu (Z.Y.), kscott@berkeley.edu (K.S.).

AUTHOR CONTRIBUTIONS

Z.Y. conceived and performed experiments and analyzed the data under guidance from K.S. Z.Y. and K.S. wrote the manuscript.

DECLARATION OF INTERESTS

The authors declare no competing interests.

SUPPLEMENTAL INFORMATION

Supplemental information can be found online at https://doi.org/10.1016/j.neuron.2021.12.028.

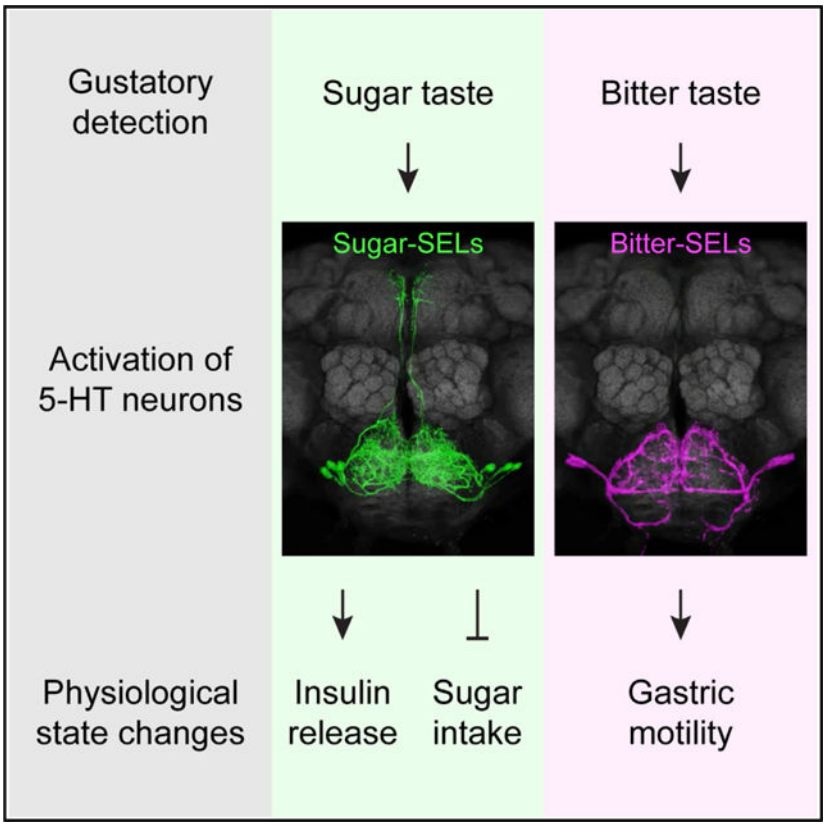

INTRODUCTION

Animals have evolved elaborate mechanisms that engage the nervous, endocrine, and digestive systems to monitor and regulate nutrient availability. Sensory systems, including the gustatory system, identify potential food sources prior to nutrient ingestion. Endocrine and digestive systems support long-term stabilization of circulating nutrients that sustain tissue and organ function. These multiple systems interact to coordinately regulate nutrient availability and maintain energy homeostasis, often across different timescales.

Seminal studies have revealed that sensory detection of food sets in motion anticipatory physiological state changes (Chen and Knight, 2016; Power and Schulkin, 2008; Zafra et al., 2006). For instance, the detection of food by the visual, olfactory, or gustatory systems influences salivation, digestive enzyme secretion, and hormone release. These sensory-evoked responses are called cephalic-phase responses, as they are elicited by the brain prior to nutritive state changes (Power and Schulkin, 2008; Zafra et al., 2006). One illustrating example is cephalic-phase insulin release in mammals. It has been known for decades that sensory detection of food triggers an initial insulin pulse that occurs before nutrients are absorbed, serving to increase glucose storage prior to blood glucose increases (Power and Schulkin, 2008; Teff, 2000; Zafra et al., 2006). Another example is anticipatory regulation of feeding-related neurons in the arcuate nucleus of the mouse hypothalamus: agouti-related peptide (AgRP) neurons are activated by hunger signals, and this hunger-related activity rapidly decreases in response to the smell or sight of food alone,

in the absence of ingestion (Betley et al., 2015; Chen and Knight, 2016; Chen et al., 2015; Mandelblat-Cerf et al., 2015). Similarly, the activity of thirst neurons in the subfornical organ is rapidly downregulated upon initiating water ingestion, prior to blood osmolality changes (Augustine et al., 2018; Zimmerman et al., 2016). A better understanding of how acute sensory detection elicits longer-term physiological changes will provide insight into the anticipatory regulation of nutrient homeostasis.

Taste detection is a key signal of nutrient availability that precedes physiological changes that accompany food intake. Gustatory detection of nutrients such as sugars precedes nutrient intake, digestion, increased circulating nutrients, and satiation. In contrast, bitter taste detection signals the presence of harmful compounds, causing food rejection, and potential nutrient deprivation. While taste detection is poised to communicate anticipated changes in nutrient status to the endocrine and digestive systems, the taste pathways that coordinate these systems remain unclear.

Drosophila, like mammals, monitors external nutrients using the gustatory system and regulates internal nutrient availability using the endocrine and digestive systems. Key features of these systems are shared in flies and mammals, including gustatory neurons tuned to sweet and bitter taste compounds (Yarmolinsky et al., 2009), and internal nutrient regulation via insulin and glucagon equivalents (Ahmad et al., 2020; Leopold and Perrimon, 2007). The numerical simplicity of the fly nervous system, the ability to monitor and manipulate single neurons, and the potentially short relays between the brain, endocrine system, and digestive tract make *Drosophila* an ideal system for examining common mechanisms underlying nutrient homeostasis.

Here, we investigate communication between the *Drosophila* gustatory system and endocrine and digestive systems and identify serotoninergic (or 5-HT, 5-hydroxytryptamine) neurons as critical circuit nodes that mediate anticipatory regulation of nutritional state. Using intersectional genetic approaches, we identified and characterized two distinct classes of 5-HT neurons that translate short-term changes in taste detection into longer-term changes in physiological state. One class of 5-HT neurons is activated by sugar taste detection prior to ingestion. These neurons excite insulin-producing neurons and limit sugar consumption, suggesting that they promote insulin release in anticipation of sugar intake and prevent overconsumption. A second class of 5-HT neurons is activated by gustatory detection of bitter compounds and activates enteric neurons that promote gastric motility. As the detection of bitter compounds signals harmful or toxic compounds, these neurons may stimulate food digestion to replenish circulating nutrients when the presence of bitter compounds prevents feeding. Together, our work reveals that 5-HT neurons anticipate nutrient availability and coordinate endocrine and digestive function for stabilization of available nutrients.

RESULTS

Sugar and bitter tastes activate distinct 5-HT neurons

Serotonin modulates appetite and food intake across animals (Tecott, 2007). The *Drosophila* central brain contains ~90 5-HT neurons (Pooryasin and Fiala, 2015), offering a tractable

model to study 5-HT neurons that modulate feeding. To examine whether *Drosophila* 5-HT neurons contribute to taste processing and feeding regulation, we first tested whether they respond to taste sensory input. The primary gustatory center of the fly brain is the subesophageal zone (SEZ), which is innervated by the axons of gustatory neurons from fly taste organs, including the proboscis, mouthparts, and legs (Stocker, 1994). Therefore, we hypothesized that 5-HT neurons in this brain region might respond to taste sensory detection.

We monitored taste-induced activity in 5-HT neurons throughout the dorsal SEZ by *in vivo* GCaMP6s calcium imaging (Chen et al., 2013; Harris et al., 2015). To selectively label 5-HT neurons, three independent Tryptophan hydroxylase (Trh) *Gal4* lines (Alekseyenko et al., 2010; Shearin et al., 2013) were used for imaging studies. The esophagus (ES) was severed to evaluate whether taste sensory stimulation activated 5-HT neurons independent of ingestion. Sucrose stimulation of proboscis gustatory neurons activated SEZ 5-HT neurons that have dense and diffuse arbors (Figures 1A–1C, upper panels). Interestingly, bitter stimulation activated different SEZ 5-HT neurons with discrete branched arborizations (Figures 1A and 1B, lower panels). Whereas two *Trh-Gal4* lines, *Trh-Gal4(S)* and *Trh-Gal4(K3)*, contained both sugar- and bitter-responding cells (Figures 1A and 1B), *Trh-Gal4(K2)* neurons responded only to sugar taste detection (Figure 1C). *Trh-Gal4(S)* and *Trh-Gal4(K3)* labeled all 5-HT neurons in the dorsal SEZ (Figures 1D and 1E). *Trh-Gal4(K2)* labeled three 5-HT neural pairs with small somas but not two 5-HT neural pairs with large somas (Figure 1F), suggesting that they are the sugar- and bitter-responding cells, respectively. These results demonstrate two distinct classes of 5-HT SEZ neurons that respond selectively to sugar or bitter taste detection.

Sugar-SELs respond to proboscis sugar detection

The taste-responsive 5-HT cells belong to the lateral subesophageal ganglion (SEL) 5-HT neural cluster (Pooryasin and Fiala, 2015); therefore, we named the sugar and bitter responding neurons as sugar-SELs and bitter-SELs, respectively. We used an intersectional genetic approach to gain specific genetic access to sugar-SELs to study their function. *Trh-Gal4*(*K2*) is expressed in sugar-SELs (Figures 1C and 1F), and the Hox-gene-based *Dfd-LexA* is expressed in all dorsal SEZ cells (Simpson, 2016). *Gal4*-dependent expression was restricted to cells containing both *Trh-Gal4*(*K2*) and *Dfd-LexA*, using flippase-mediated excision of *Gal80* (Gordon and Scott, 2009). This intersectional strategy restricted *Gal4* activity specifically to the sugar-SELs (Figures 2A–2C; Video S1; STAR Methods).

Sugar-SELs consist of three neural pairs with both dendritic (marked by DenMark; Nicolaï et al., 2010) and axonal (marked by Syt-GFP; Zhang et al., 2002) arbors in the SEZ (Figures 2A-2E), consistent with a role in taste processing. In addition, sugar-SELs send axonal projections along the median bundle to the pars intercerebralis (PI) (Figure 2E), a neuroendocrine center. Single-cell labeling approaches (Hampel et al., 2011) revealed three sugar-SEL morphological subtypes: an ipsilateral projection neuron (PN) (Figure S1A), a contralateral PN (Figure S1B), and a SEZ local neuron (LN) (Figure S1C). An SEZ *split-Gal4* collection contained two *split-Gal4* lines targeting sugar-SEL PNs and LNs, respectively (Figures S1D and S1E′; Sterne et al., 2021). Sugar-SEL PNs have dendrites

and axons in the SEZ and axons in the PI (Figures S1F and S1F0). Sugar-SEL LNs have dendrites and axons in the SEZ (Figure S1G).

We confirmed that sugar-SELs respond to sugar taste detection on the proboscis but not bitter detection (Figures 2F–2K). Calcium responses were detected in SEZ arbors (Figures 2F–2H) and median bundle projections (Figures 2I–2K), using flies with GCaMP6s expressed in all sugar-SELs. Using specific *split-Gal4* lines that distinguish the sugar-SEL PNs and LNs, we found that both cell populations responded to sugar taste detection (Figures S1H–S1K). Optogenetic excitation of sugar (*Gr64c*$^{+}$) gustatory receptor neurons (GRNs) but not bitter (*Gr66a*$^{+}$) GRNs (Freeman and Dahanukar, 2015), using the light-gated channel CsChrimson (Klapoetke et al., 2014), also activated sugar-SEL PNs (Figures 2L–2N, S1L, and S1M). Furthermore, we found that proboscis sensory input is critical for the response, as severing the pharyngeal nerve, conveying internal mouthparts GRN axons, did not affect the sugar-SEL response, whereas severing both the pharyngeal nerve and the labial nerve (LN), conveying proboscis labellar GRNs, abolished the response (Figures S1N and S1O). Interestingly, sugar-SELs responded to sugar stimulation of proboscis GRNs but not leg GRNs (Figures 2O–2Q), suggesting that sugar-SELs may participate in feeding rather than food searching.

Sugar-SELs excite insulin-producing cells

Sugar-SEL PNs send axons to the PI (Figures S1A, S1B, S1D, and S1F0), raising the intriguing possibility that they regulate neuroendocrine function. The PI contains many neurosecretory cells, including insulin-producing cells (IPCs) that secrete *Drosophila* insulin-like peptides (DILPs) and regulate sugar metabolism, akin to mammalian pancreatic β cells (Ahmad et al., 2020; Leopold and Perrimon, 2007). Neurites of sugar-SEL PNs and IPCs overlap extensively in the SEZ, the median bundle, and the PI (Figures 3A–3C and S2A), suggesting potential synaptic connections.

We examined 5-HT receptor expression in IPCs using knockin *Gal4* lines (Gnerer et al., 2015) to test whether IPCs might directly detect sugar-SEL 5-HT release. Of the five *Drosophila* 5-HT receptors, only 5-HT2A is expressed in five to six (5.67 ± 0.21, mean ± SEM, n = 6 brains) IPCs, albeit at low levels (Figures 3D–3F and S2B–S2F"). 5-HT2A is an excitatory 5-HT receptor (Vleugels et al., 2015), suggesting that IPCs are activated by sugar-SEL PNs. Consistent with this hypothesis, we found that IPCs responded to sugar taste detection (Figures 3G–3I), similar to sugar-SELs. The response persisted in flies with the ES severed (Figures S2G–S2I), indicating that the response was independent of ingestion. This is reminiscent of the cephalic phase insulin response in mammals, where insulin is secreted in response to sensory detection of food well before blood glucose levels change (Power and Schulkin, 2008; Teff, 2000; Zafra et al., 2006). In contrast, Diuretic hormone 44 (Dh44) neurons in the PI, which sense circulating glucose (Dus et al., 2015), showed small, delayed, and variable responses to sugar taste detection (Figures S2J–S2L).

To test whether 5-HT2A is required in IPCs for the sugar response, we knocked down *5-HT2A* expression in IPCs and found that this reduced but did not abolish the response (Figures S2M and S2N), arguing that 5-HT2A contributes to the activation of IPCs but that RNAi knockdown is incomplete and/or additional pathways exist. Consistent with this, when

we applied mianserin, an antagonist of *Drosophila* 5-HT2 receptor subtypes (Blenau et al., 2017; Colas et al., 1995; Tierney, 2018; Vleugels et al., 2015), to the exposed fly brain, taste-evoked calcium responses in IPCs were diminished (Figures 3H–3J).

To directly test the hypothesis that sugar-SEL PNs excite IPCs, we activated sugar-SEL PNs using CsChrimson, while simultaneously monitoring the response in IPCs (Figure 3K). Optogenetic activation of sugar-SEL PNs excited IPCs, demonstrating an excitatory connection (Figures 3L–3N). This response was largely inhibited in the presence of mianserin (Figures 3L-3N), consistent with a requirement for 5-HT signaling. Furthermore, optogenetic excitation of sugar-SEL PNs decreased cytoplasmic Dilp2 levels (Figure S2P), consistent with sugar-SEL PN activity promoting pre-absorptive Dilp2 release. In contrast, sugar-SEL LNs have little anatomical overlap with IPCs (Figures 3O and 3P), and optogenetic activation of sugar-SEL LNs did not consistently excite IPCs (Figures 3Q and 3R). Taken together, these results indicate that sugar-SEL PNs relay sugar taste detection to IPCs to promote insulin release, likely in anticipation of sugar consumption.

Sugar-SELs limit sugar consumption

The findings that sugar-SELs respond to sugar taste detection on the proboscis but not on the legs (Figures 2O–2Q) and that they activate IPCs (Figures 3K–3N) suggest that they regulate feeding. To test this, we measured sugar intake in fasted flies, using a temporal consumption assay (Joseph et al., 2017; Pool et al., 2014). Transient excitation of sugar-SELs using the heat-activated cation channel dTRPA1 (Hamada et al., 2008) decreased sugar consumption (Figures 4A and 4B). In contrast, transient inhibition of synaptic transmission in sugar-SELs by overexpressing a dominant-negative, temperature-sensitive Dynamin (Shi^{ts}) (Kitamoto, 2001), increased sugar consumption (Figures 4C and 4D). Importantly, blocking 5-HT synthesis in sugar-SELs, by specific expression of *Trh* RNAi, also increased sugar consumption (Figure 4E). These findings demonstrate that 5-HT output from sugar-SELs limits sugar intake.

Given that sugar-SEL PNs and LNs have different anatomy and functional connectivity to IPCs (Figures 3K–3R and S1A–S1G), we examined whether they differentially regulate sugar consumption. Optogenetic excitation of sugar-SEL PNs decreased sugar consumption, whereas excitation of sugar-SEL LNs had no measurable effect (Figure 4F). However, hyperpolarizing either sugar-SEL PNs or LNs using the light-gated anion channel GtACR1 (Mohammad et al., 2017) increased sugar consumption (Figure 4G), suggesting that sugar-SEL PNs and LNs cooperate to limit sugar consumption.

Given that IPCs promote satiety, e.g., through the neuropeptide Drosulfakinin (Söderberg et al., 2012; Wang et al., 2020), we wondered if sugar-SELs act through the IPCs to limit consumption. While the knockdown of *5-HT2A* expression in IPCs reduced their taste-evoked response (Figures S2M and S2N), it had no effect on sugar consumption (Figure S2O). More importantly, we found that activation of sugar-SEL PNs suppressed sugar consumption in animals with IPCs silenced (Figure 4H), demonstrating that sugar-SEL PNs are able to inhibit consumption via a pathway not requiring IPCs. Taken together, our studies demonstrate that activation of sugar-SELs by sugar gustatory detection increases IPC activity and independently decreases consumption (Figure 4I), providing insight into the

neural circuit that regulates internal nutrient availability and consumption in anticipation of sugar intake.

Bitter-SELs respond to bitter taste detection

We next examined the role of bitter-SELs in gustatory processing and feeding regulation. The distinct morphology of bitter-SELs (Figures 1A and 1B, lower panels) allowed us to visually identify a *Gal4* driver, *VT46202-Gal4*, that labels them. *VT46202-Gal4* has sparse expression in the central brain, labeling only the bitter-SELs in the SEZ (Figures S3A and S3A′). The genetic intersection of *VT46202-Gal4* and *Dfd-LexA*, using *LexAop-FLP* and *tub-FRT-Gal80-FRT*, restricted *Gal4*-dependent expression to bitter-SELs (Figures 5A and 5B; Video S1). Bitter-SELs arborize in the SEZ and send descending processes that arborize on the dorsal surface of the ventral nerve cord (VNC) (Figures 5A-5C′). This morphology identified bitter-SELs as DNg28 descending neurons (DN) in the DN *split-Gal4* collection (Namiki et al., 2018) (Figures S3B and S3B′). The dendrites of bitter-SELs are largely restricted to the SEZ, consistent with receiving taste input, and the descending projections are axonal (Figure 5D).

Using specific drivers to express GCaMP6s in bitter-SELs, we confirmed that they responded to bitter taste detection on the proboscis (Figures 5E–5G), consistent with the *Trh-Gal4* studies (Figures 1A and 1B). Moreover, bitter-SELs were activated by optogenetic excitation of bitter (*Gr66a*$^{+}$) but not sugar (*Gr64c*$^{+}$) GRNs (Figures 5H–5J). In contrast to the specific response of sugar-SELs to proboscis sugar detection (Figures 2O–2Q), bitter-SELs responded to bitter detection on both the proboscis and legs (Figures 5K–5M). These findings suggest that bitter-SELs may play a general role in bitter taste detection rather than a specific role in regulating consumption. Indeed, neither exciting or silencing bitter-SELs had a measurable effect on consumption of sugar or sugar-bitter mixtures (Figures S3D, S3E, and S3G–S3I).

Bitter-SELs excite 5-HT7 enteric neurons

In addition to arborizations in the central nervous system, bitter-SELs have processes associated with the digestive system. Bitter-SELs send projections through the LNs and through the recurrent nerve (RN) to the hypocerebral ganglion (HCG) (Figures 6A–6D, S4A, and S4B). Interestingly, bitter-SEL projections appear to account for all 5-HT processes innervating the HCG (Figures 6E–6E"). The HCG is an enteric ganglion at the junction of the ES, crop (food storage), and proventriculus (PV)/anterior midgut (food grinding and digestion) (Figure 6A; Lemaitre and Miguel-Aliaga, 2013; Miguel-Aliaga et al., 2018). This junction region is a key site for the regulation of food passage to the crop for temporary storage or the midgut for digestion. The anatomy of bitter-SEL projections suggests the hypothesis that they participate in the regulation of digestion.

To examine the possibility that bitter-SELs synapse onto enteric neurons in the proventricular region and regulate digestion, we first examined the expression of 5-HT receptors in this region using knockin *Gal4* lines (Gnerer et al., 2015). Of the five 5-HT receptors, the excitatory 5-HT receptor 5-HT7 is expressed abundantly in the proventricular region (Figures S4C-S4G"), in processes innervating the proventriculus/anterior midgut and

the crop (Figures 6F and S4G′), and thus is well positioned to receive 5-HT input from bitter-SELs (Figures 6E and 6F). Consistent with this, we found that optogenetic excitation of bitter-SELs induced calcium increases in 5-HT7(+) enteric processes, demonstrating an excitatory connection (Figures 6G–6I). In contrast, nearby adipokinetic hormone (AKH) cells did not express 5-HT receptors (Figures S4C-S4G") and were not consistently activated by optogenetic excitation of bitter-SELs (Figures S4H–S4J). In summary, bitter-SELs innervate the HCG and excite 5-HT7(+) enteric neurons in the proventricular region, suggesting that they regulate enteric physiology and function.

Bitter-SELs promote crop contractions through 5-HT7

5-HT modulates gastrointestinal motility in mammals and insects (Tecott, 2007). In insects including *Drosophila*, 5-HT promotes crop (food storage organ) contractions (e.g., Calkins et al., 2017; French et al., 2014; Liscia et al., 2012; Solari et al., 2017); however, the source of 5-HT and the underlying 5-HT receptors are unknown. Our finding that bitter-SELs project to the HCG and excite 5-HT7(+) enteric neurons (Figure 6) suggests that bitter-SELs may supply 5-HT to the digestive tract to modulate crop contractions via 5-HT7(+) enteric neurons. To test this, we developed a preparation to observe crop contractions in live flies that is compatible with simultaneous optogenetic stimulation (Figure 7A; STAR Methods).

We found that optogenetic excitation of bitter-SELs using CsChrimson increased crop contractions (Figures 7B and 7C; Video S2). Optogenetic excitation of bitter GRNs also slightly increased crop contractions (Figures 7D and 7E). Similarly, when 5-HT7(+) neurons were activated using the light-gated cation channel ReaChR (Inagaki et al., 2014; Lin et al., 2013) (because CsChrimson expression induced lethality), crop contractions increased and were sustained for tens of seconds post-stimulation (Figures 7F and 7G). To test if 5-HT7 is required for bitter-SELs to promote crop contractions, we optogenetically excited bitter-SELs using the *R24F06-LexA* driver (Figures S3C and S3C′) in a *5-HT7* heterozygous or homozygous null mutant background (Qian et al., 2017). The homozygous null mutation of *5-HT7* largely suppressed bitter-SEL-induced crop contractions (Figures 7H and 7I). Together, these studies show that bitter-SELs act through 5-HT7 in enteric targets to promote crop contractions (Figure 7J). As regurgitation was not observed when bitter-SELs were excited in the consumption assay (Figures S3D and S3E), these results suggest that bitter-SEL excitation promotes the movement of food from the crop into the midgut for digestion. Interestingly, activation of bitter-SELs did not alter the excretion rate (Figure S3F), which may suggest increased absorption. Taken together, our findings suggest the model that in the presence of bitter and thus potentially harmful substances, bitter-SELs activate 5-HT7(+) enteric neurons to promote crop contractions, likely to utilize food reserves for energy replenishment in anticipation of potential food shortages (Figure 7J). Thus, our studies show that both sugar-SELs and bitter-SELs transform taste detection into anticipatory regulation of internal nutrient availability.

DISCUSSION

In this study, we identified two classes of 5-HT neurons that play distinct roles in gustatory processing and function independently to promote nutrient homeostasis. Sugar-

SELs respond to sugar gustatory detection, promote IPC activity, and reduce feeding drive, suggesting that they prevent overconsumption in nutrient rich environments. Bitter-SELs respond to bitter taste detection and promote crop contractions, likely to utilize stored food upon food rejection. Thus, 5-HT neurons coordinate endocrine and digestive function in anticipation of altered food intake.

5-HT regulates feeding and nutrient homeostasis

5-HT profoundly modulates appetite and feeding across animal species (Tecott, 2007). In humans and rodents, the global effect of brain 5-HT signaling is suppression of food intake; however, the involvement of multiple brain regions (including the hypothalamus, solitary tract nucleus, and parabrachial nuclei) and multiple 5-HT receptors (e.g., 5-HT1B, 5-HT2C, 5-HT6) underscores the complex nature of 5-HT modulation of appetite and feeding (Donovan and Tecott, 2013; Lam et al., 2010; Marston et al., 2011; Tecott, 2007; Wyler et al., 2017). Studies in invertebrates have likewise demonstrated multiple, sometimes opposite, roles for 5-HT neurons in regulating feeding (Tierney, 2020). For instance, in *Drosophila* adults, activating all 5-HT neurons suppresses food intake whereas activating a smaller yet diverse subset promotes food intake, suggesting heterogeneity in 5-HT feeding regulation (Albin et al., 2015; Pooryasin and Fiala, 2015). With the exception of a few cases where specific 5-HT neurons that influence feeding have been identified–for example, 5-HT neurons that promote pharyngeal pumping to enhance ingestion in *C. elegans* and *Drosophila* larvae (Ishita et al., 2020; Schoofs et al., 2018; Tierney, 2020)–the diversity of 5-HT neurons that contributes to feeding regulation and nutrient homeostasis remains largely uncharacterized.

Here, we identify multiple classes of 5-HT neurons that are activated by gustatory detection and signal to the endocrine and digestive systems to influence nutrient availability. Our studies reveal 5-HT neurons that have different projection patterns, relay sugar and bitter gustatory information to different downstream targets, and regulate internal nutrient availability by distinct mechanisms. These studies provide insight into the multifaceted roles of 5-HT neurons in gustatory processing, feeding regulation, and nutrient homeostasis, highlighting the importance of understanding the myriad functions of 5-HT at the neural circuit level.

Sugar taste detection regulates insulin release and feeding drive

Food-derived sensory cues are used as anticipatory signals to regulate endocrine function and feeding drive. Work in mammals has demonstrated that there are two phases of insulin release in response to food consumption, a pre-absorptive phase in response to sensory detection of food and a post-absorptive phase in response to elevated blood glucose levels. The pre-absorptive phase (cephalic phase) is triggered by sensory detection prior to food consumption and nutrient absorption (Power and Schulkin, 2008; Teff, 2000; Zafra et al., 2006). The neural circuit that underlies pre-absorptive insulin release, however, is not fully understood.

Our findings suggest that insulin release in anticipation of food consumption is a process shared in flies and mammals, perhaps indicating an effective strategy to promote rapid

nutrient storage during feeding. Using *in vivo* calcium imaging, we found that fly IPCs are rapidly excited by sugar gustatory detection independent of consumption (Figures 3G–3J and S2G–S2I). Our findings that sugar-SELs respond to sugar taste detection and activate IPCs suggest a neural circuit mechanism for pre-absorptive insulin release independent of ingestion. Moreover, as gustatory sensory neurons detect both nutritive and non-nutritive sugars (Fujita and Tanimura, 2011) and are inputs to sugar-SELs and IPCs, we anticipate that sugar-SELs, IPCs, and pre-absorptive insulin release are also activated by non-nutritive sugars, but this requires further investigation. Our finding that fly IPCs are activated by sugar taste detection contrasts with our previous whole-brain imaging studies (Harris et al., 2015), likely indicating signal detection limits. Here, in addition to identifying sugar taste responses in IPCs, we also identified the sugar-SELs as a specific neural pathway mediating the preparatory insulin response (Figure 3).

We find that knocking down *5-HT2A* in IPCs reduces but does not abolish gustatory-induced IPC activity and does not impact consumption. One caveat of this approach is that RNAi reduces gene expression and may not produce complete loss-of-function phenotypes. The IPCs are activated by many nutritional state signals, including multiple pathways that report circulating sugars and signals from the intestine and fat body (Nässel and Zandawala, 2020). Our work shows that external nutrients in the form of sugar taste detection also activate this important hub and identifies sugar-SELs as a defined pathway conveying the sugar taste signal. As IPCs release multiple peptides, the activation of IPCs by sugar-SELs may coordinate widespread changes in metabolism and behavior. Thus, we have identified a specific class of 5-HT neurons that participates in the preparatory insulin response and the reduction of feeding drive in response to sugar gustatory detection, shedding light on the neural circuit mechanisms that anticipate sugar consumption.

Bitter gustatory detection may predict food scarcity

A surprising finding from our study is that bitter-SELs, which respond to bitter gustatory detection, promote contractions of the crop food storage organ. While there is evidence that intestinal bitter detection modulates gastrointestinal physiology (Sarnelli et al., 2019; Xie et al., 2018), the regulation of gastrointestinal function by bitter gustatory detection is less examined. We find that activation of bitter gustatory neurons, bitter-SELs, and 5-HT7 neurons all promote crop contractions, although rates differ, possibly based on optogenetic activation strength or propagation of activity to the crop.

Why do bitter compounds promote crop contractions? We reason that because bitter compounds are feeding deterrents, frequent encounters with bitter compounds may prevent food intake, leading to depletion of internal nutrients. Under such conditions, bitter-SELs may promote crop motility to utilize food reserves in anticipation of limited food intake. We therefore propose that bitter gustatory compounds may have an unappreciated role in predicting food scarcity and stimulating digestion as a preparatory response.

Previous studies in *Drosophila* have demonstrated that bitter taste detection elicits inhibition of proboscis extension and suppression of consumption (Keene and Masek, 2012; Marella et al., 2006; Meunier et al., 2003; Thorne et al., 2004; Wang et al., 2004). In addition, detection of bitter compounds drives avoidance behavior and increased locomotion, likely

to promote departure to new areas (Hernandez-Nunez et al., 2015; Meda et al., 2020). Our findings suggest an additional role for bitter taste detection in promoting mobilization of food stores to increase circulating nutrients. These actions are aligned in mitigating the impact of a potentially toxic food source by limiting consumption, promoting relocation, and maintaining internal nutrient levels. Whereas bitter taste detection rapidly leads to consumption inhibition and increased locomotion, whether bitter taste detection activates crop contractions acutely or only under specific conditions of food deprivation is not resolved. In addition, although we observed increased crop contractions upon activation of bitter-SELs, it remains to be examined whether this impacts internal circulating nutrients. Bitter-SELs may also influence additional aspects of feeding behavior not tested here, including modulating consumption under different physiological states or when different feeding assays or different bitter compounds are used.

In addition to the HCG, bitter-SELs project to diverse targets (Figures 6B–6D, S4A, and S4B), suggesting that they may carry out other functions besides enteric modulation. For example, bitter-SELs broadly arborize on the dorsal surface of the VNC (Figures 5C, 5C′, and S4A; Namiki et al., 2018). Thus, bitter-SELs may also set the 5-HT tone in the VNC or secrete 5-HT into the hemolymph to modulate target tissues in a paracrine or endocrine fashion.

Neuromodulatory circuits as candidates for mediating preparatory responses

We find that 5-HT neurons are critical nodes in the circuits that transform gustatory detection into changes in endocrine and digestive function. Although the timescale of activation of sugar-SELs and bitter-SELs and the dynamics of 5-HT release requires further investigation, 5-HT receptors are metabotropic receptors ideally suited for transforming transient neural signals into more sustained cellular responses. In this regard, neuromodulatory circuits are prime candidates for eliciting preparatory responses that require the transformation of neural signals across time scales. Our work thus sheds light on neural circuit mechanisms that translate external sensory cues into preparatory physiological responses and suggests that neuromodulators such as 5-HT may contribute to anticipatory mechanisms in other animals.

STAR★METHODS

RESOURCE AVAILABILITY

Lead contact—Further information and requests for resources and reagents should be directed to and will be fulfilled by the lead contact, Kristin Scott (kscott@berkeley.edu).

Materials availability—All materials generated in this study including fly lines and custom apparatus will be available upon request.

Data and code availability

- Data reported in this paper will be shared by the lead contact upon request.
- All original code has been deposited at Zenodo and is publicly available as of the date of publication. The DOI is listed in the key resources table.

- Any additional information required to reanalyze the data reported in this paper is available from the lead contact upon request.

EXPERIMENTAL MODEL AND SUBJECT DETAILS

All experiments were performed in the fruit fly *Drosophila melanogaster*. The key resources table lists the transgenic lines used in this study and Table S1 documents the genotypes used for each figure. Flies were reared on standard cornmeal-yeast-molasses media at 25°C with 65% humidity and a 12hr: 12hr light: dark cycle unless stated otherwise. Flies for optogenetic experiments were raised on standard food and in darkness. Upon eclosion, adult flies were collected and maintained on standard food supplemented with 400 μM all-trans-retinal and in darkness prior to experiments. Flies for dTRPA1, Shi^{ts}, and Brainbow experiments were raised at 20–22°C. Adult mated female flies were used for all experiments.

METHOD DETAILS

Genetic intersections—We used two different intersectional genetic approaches to refine driver expression. The first approach was a genetic intersection between a *Gal4* driver (Brand and Perrimon, 1993; Fischer et al., 1988) and a *LexA* driver (Lai and Lee, 2006). A ubiquitously expressed *Gal80* flanked by two flippase recognition target (*FRT*) sites (i.e., *tub-FRT-Gal80-FRT* [Gordon and Scott, 2009]) was used to suppress *Gal4/UAS* expression. A *LexA* driver was used to express flippase (FLP), which excised the *Gal80* hence allowing *Gal4/UAS* expression. As a result, only cells expressing both *Gal4* and *LexA* expressed the *UAS* transgene. The second approach was the *split-Gal4* strategy (Luan et al., 2006). The activation domain of p65 (p65.AD) and the DNA-binding domain of Gal4 (Gal4.DBD) were driven by two different enhancers (Pfeiffer et al., 2010). A functional Gal4-p65 hybrid transcription factor was reconstituted only in cells expressing both enhancers.

Calcium imaging with taste stimulation—*In vivo* calcium imaging with taste stimulation was performed as previously described (Harris et al., 2015; Kim et al., 2017). Mated female flies, 5–14 day old, were food-deprived on a piece of wet kimwipe for ~24 hours prior to imaging. An individual fly was briefly anesthetized using CO_2 and gently placed into a small slit on a custom-built plastic mount at the cervix so that the head was above the plastic mount while the body was beneath it. The head was then immobilized using nail polish, and the proboscis was gently pulled out using a suction glass pipette and waxed at the rostrum and maxillary palps so that it was in an extended position to allow for taste solution delivery. A piece of coverslip was placed at the base of the rostrum at a 45° angle to the plane of the plastic mount to separate the proboscis from the head. The head was then submerged in adult hemolymph-like (AHL) saline containing 108 mM NaCl, 5 mM KCl, 2 mM $CaCl_2$, 2 mM $MgCl_2$, 4 mM $NaHCO_3$, 1 mM NaH_2PO_4, 5 mM trehalose, 10 mM sucrose, 5 mM HEPES (pH 7.5) (Wang et al., 2003). For subesophageal zone (SEZ) imaging, the antennae, the head cuticle above the SEZ, and the underlying air sacs were removed using fine forceps. The esophagus was severed to allow better optical access to the SEZ, except for Figures 5K–5M. For imaging of the median bundle and insulin-producing cells (Figures 2I–2K, 3H–3J, and S2G–S2N), additional cuticle was removed to expose

the imaged regions. The esophagus was severed for Figures S2G–S2I, and kept intact for Figures 2I–2K, 3H–3J, and S2J–S2N.

All calcium imaging experiments involving taste stimulation were performed on a fixed-stage Intelligent Imaging Innovations (3i) spinning disk confocal microscope equipped with a Zeiss Plan-APOCHROMAT 20×/1.0 water objective at 1.6× or 1.25× optical zoom. The microscope was equipped with a Piezo drive allowing rapid volumetric scanning. GCaMP6s signal was imaged with a 488 nm laser for 8–14 z-planes encompassing the cells of interest (1.0–1.5 μm steps, 50–100 ms exposure for each plane) at an interval of 1.5–2.0 seconds for 30–60 time-points, using the SlideBook6 acquisition software. Taste stimulation to the proboscis was delivered using a glass capillary (1.0 mm OD/ 0.58 mm ID) filled with ~5 μL of taste solution. The solution was drawn up the capillary slightly using suction generated by a 1 mL syringe, so that the tip of the capillary was empty. The capillary was then placed over the proboscis using a micromanipulator, visualized under a USB microscope camera. Slight pressure was applied to the syringe to deliver taste solution to the proboscis at desired time-points. To deliver taste stimulation to the legs, a 200 μL pipette tip was attached to a 1 mL syringe and filled with taste solution, and these were secured horizontallyon a micromanipulator. A drop of taste solution (~10 μL) was suspended on the tip of the pipette tip, which was cut to wedge-shaped, and placed in front of the fly prior to image acquisition. The taste solution droplet was manually advanced to contact the legs of the fly at desired time-points, visualized under a USB microscope camera. Sugar solution contained 1 M sucrose, and bitter solution contained 100 mM caffeine, 10 mM denatonium, and 20% polyethylene glycol (PEG). For experiments only involving proboscis taste stimulation (Figures 1A–1C, 2F–2K, 3H–3J, 5E–5G, S1H–S1K, S1N, S1O, and S2G-S2N), legs were removed. For experiments involving both leg and proboscis taste stimulations (Figures 2O–2Q and 5K–5M), legs were kept intact. For experiments involving cutting the pharyngeal nerves and labial nerves (Figures S1N and S1O), the sugar-SEL response to sucrose was first imaged with both sets of nerves intact, then imaged again after the pharyngeal nerves were severed using fine forceps, then imaged for a third time after the labial nerves were severed. For experiments with mianserin (Figures 3H-3J), the insulin-producing cells were first imaged in AHL saline, then AHL saline was replaced by AHL saline supplemented with 100 μM mianserin hydrochloride, and the insulin-producing cells were re-imaged ~10 minutes later.

Calcium imaging with optogenetics—*In vivo* calcium imaging with optogenetic stimulation was performed on a Zeiss LSM 880 NLO AxioExaminer equipped with a Coherent Chameleon laser and a Zeiss Plan-APOCHROMAT 20×/1.0 water objective. For imaging of sugar-SELs, bitter-SELs, and insulin-producing cells (Figures 2L–2N, 3K–3N, 3Q, 3R, and 5H–5J), flies were prepared for imaging as described above, except that flies were not food-deprived and their legs were intact. For imaging of 5-HT7(+) enteric neurons and AKH cells (Figures 6G–6I and S4H–S4J), flies were mounted on a recording chamber as described in (Murthy and Turner, 2013), with the dorsal head and thorax accessible for dissection and imaging. The transgene *Act88F:Rpr* in these flies (see Table S1) ablated the indirect flight muscles that fill most of the thorax (Chen et al., 2018), allowing direct optical access to the proventricular region after the dorsal thoracic cuticle and the underlying

air sacs and residual muscles were removed using fine forceps. GCaMP6s was imaged on a single plane at 1 Hz with 920 nm 2-photon excitation except for that of the 5-HT7(+) enteric neurons (Figures 6G–6I), which was imaged with a 488 nm laser (at very low intensity, 0.15–0.20%) in order to obtain a thicker z-section to minimize movement artifacts. Optogenetic stimulation was delivered by a mercury lamp filtered at 650 nm (as described in (Bidaye et al., 2020)) or a custom-made 660 nm red diode laser controlled by a pulse generator for 2 s ON and 60 s OFF for three cycles. We used *Gr64c-LexA* to drive *CsChrimson* expression in the sugar GRNs (Figures 2L–2N and 5H–5J) because it does not drive expression in the antennal lobes, in contrast to *Gr5a-LexA* and *Gr64f-LexA* (Figure S1L) (Fujii et al., 2015). Mianserin was applied as described above.

Immunohistochemistry—Antibody staining of whole-mount *Drosophila* brain and other tissues was performed as previously described (Yao and Shafer, 2014) with minor modifications. Fly heads (for brain-only staining) or whole flies, with cuticles gently torn open using forceps, were fixed in 3% paraformaldehyde in phosphate buffered saline (PBS) for 1 hr at room temperature. After three washes in PBS, tissues of interest (brain, brain + VNC, guts, or brain + VNC + guts) were dissected in PBS then transferred to PBST (PBS with 0.3% Triton X-100). Tissues were blocked with 5% normal goat serum in PBST for 1 hr at room temperature, then incubated with primary antibodies in block solution at 4°C for 2–3 days. After five 15-min washes in PBST, tissues were incubated with secondary antibodies in block solution at 4°C for 1–2 days. After five 15-min washes in PBST, followed by 1–2 exchanges of PBS, tissues were mounted on poly-L-lysine-coated coverslips in PBS and dehydrated in a graded glycerol series (30%, 50%, and 70% glycerol in PBS for 5 min each). The final glycerol solution was replaced with Vectashield Antifade Mounting Medium (H-1000) for imaging and storage. The stained tissues were imaged under a Zeiss LSM 780 or LSM 880 AxioExaminer equipped with a Zeiss Plan-APOCHROMAT 20×/1.0 water objective and a Zeiss Plan-APOCHROMAT 40×/1.0 water objective, using excitation and emission wavelengths corresponding to those of the fluorophores conjugated to the secondary antibodies. Image brightness and contrast were adjusted using Fiji/ImageJ, and image stitching was performed using the Pairwise Stitching plugin in Fiji/ImageJ. For the immunostaining of Dilp2 (Figure S2P), flies with CsChrimson expression in sugar-SEL PNs and genetic controls were food-deprived in a clear plastic vial with a piece of wet kimwipe for ~24 hours in darkness, then placed in a box with red LEDs flashing 1 second ON and 0.5 second OFF for 1.5 hours, controlled by an Arduino UNO board. After that, flies were immediately placed on ice and subjected to the antibody staining procedure. The same imaging acquisition settings were used for the experimental and control groups of Dilp2 immunostaining. Antibodies and their dilutions are described in the key resources table.

Analysis of single-cell morphology—We used the *Drosophila* Brainbow technique (Hampel et al., 2011) to analyze the single-cell morphology of sugar-SELs. We initially analyzed the morphology of single sugar-SELs using the genetic intersection of *Trh-Gal4.long(2)* and *Dfd-LexA*. We repeated the analysis using *split-Gal4s* for the sugar-SEL PNs (*SEZ-205*) and sugar-SEL LNs (*SEZ-569*) and co-stained for 5-HT (Figures S1A-S1C; Table S1). Flies were raised at 20–22°C without heat shock (because *Crey(1b)* expressed Cre

recombinase constitutively), and brains from 7–11 day old mated females were dissected for immunohistochemistry for single-cell morphology analysis.

Image registration to template brain—Confocal image stacks of sugar-SELs and bitter-SELs in separate brains were aligned to the brain template JFRC2 (available at https://github.com/jefferislab/BridgingRegistrations) using the anti-Brp (nc82) staining as a reference channel, by nonrigid warping using the Computational Morphometry Toolkit (CMTK) (https://www.nitrc.org/projects/cmtk/), as described in detail in (Jefferis et al., 2007). The registered sugar-SEL and bitter-SEL images, and the JFRC2 brain template were visualized and 3D rendered using FluoRender (https://www.sci.utah.edu/software/fluorender.html) (Video S1).

Temporal consumption assay—Temporal consumption assay was performed similarly to previously described (Pool et al., 2014). Adult mated female flies, 6–15 day old, were food-deprived on a piece of wet kimwipe for ~24 hours (unless stated otherwise). Flies were mounted on glass slides with nail polish and allowed to recover in a humidified chamber for ~2–3 hours. Individual flies were presented with a drop of 1 M sucrose or a mixture of 1 M sucrose and the indicated bitter compounds (supplemented with 0.25 mg/mL FD&C No. 1 blue dye for visualization) from a 200 μL pipette tip attached to a 1 mL syringe and allowed to consume for at least 10 times and until the flies no longer consumed. Feeding bouts were video recorded at 30 frames per second using a USB microscope camera and manually annotated (Figures 4A–4E) or manually recorded using an online chronometer (http://online-stopwatch.chronme.com/) (Figures 4F–4H, S2O, S3D, S3E, and S3G–S3I). Flies for dTRPA1 and Shi^{ts} experiments were raised 20–22°C. To activate dTRPA1, flies were placed on a 29–30°C heat block for at least 5 min before testing and throughout testing. For Shi^{ts} silencing experiments, flies were placed in a humidified chamber at 30–32°C for ~2–3 hours and then tested on a 30–32°C heat block. Sibling controls from the same genetic crosses were used for both sets of experiments (except for Figure 4H). Flies for CsChrimson and GtACR1 experiments were raised on standard food at 25°C in darkness. Upon eclosion, adult flies were collected and maintained on standard food supplemented with 400 μM all-trans-retinal until they were food-deprived for the consumption assay. CsChrimson was activated by a Laserglow red laser (635–650 nm) and GtACR1 was activated by a Laserglow green laser (532 nm) for ~1 min before testing and during testing.

Defecation assay—Defecation assay was performed similarly to previously described (Cognigni et al., 2011; Wayland et al., 2014). Mated female flies were kept on standard food supplemented with 5 g/L Bromophenol Blue sodium salt (BPB) for at least two days prior to the defecation assay. Groups of 6–8 flies were introduced into a 35 mm petri dish with a small cube of BPB food and allowed to feed and excrete for 24 hours. The flies and food were then removed from the dish and a high-resolution image of the fecal deposits left on the petri dish lid and bottom was acquired using a HP Deskjet F4180 scanner. The number of fecal deposits was counted using The Ultimate Reader of Dung software (https://sourceforge.net/projects/the-ultimate-reader-of-dung/) as described (Wayland et al., 2014). Image cropping and preparation were done in Fiji/ImageJ. Statistical tests were performed in Prism and reported in the figure legends.

Crop contraction assay—The crop contraction assay was modified from Solari et al. (2017). We used flies fed *ad libitum* on fresh food for 3–5 days because they typically had few basal crop contractions. A live fly was briefly anesthetized with ice and mounted on the bottom of a 35 mm petri dish using petroleum jelly with its ventral side facing up. The legs were removed (except for Figures 7D and 7E), the proboscis was sealed with wax, and AHL saline was added to the dish to submerge the fly. The cuticle in the ventral upper abdomen was torn open using fine forceps with care not to damage the crop or gut tissues, exposing the crop for video recording. The above procedures were carried out at low light intensity, and the fly was allowed to recover in darkness for ~3–5 min before recording began. Crop contractions were video recorded under 850 nm infrared light illumination at 10 frames per second, using a FLIR Blackfly S USB3 camera (BFS-U3–13Y3M) mounted on an Olympus SZX16 stereo microscope. Optogenetic stimulation was delivered by a custom-made 630 nm LED panel controlled by a pulse generator (100 Hz of 5 ms pulses for 30 s). A 760 nm longpass filter was fitted in front of the camera to prevent the 630 nm stimulation light from interfering with video recording (Figure 7A).

QUANTIFICATION AND STATISTICAL ANALYSIS—All statistical tests were performed in Prism. Data was tested for normal distribution using the D'Agostino & Pearson normality test. In general, if all data for comparison passed the normality test (alpha = 0.05), parametric tests were used; otherwise, nonparametric tests were used. For similar experiments, the same statistical tests were performed for consistency.

Calcium imaging with taste stimulation—The volumetric GCaMP6s images for taste stimulation experiments were collapsed in the z-axis to generate a max-intensity z-projection image (referred to as max-z image hereafter) for each time-point. This max-z image sequence was corrected for movement artifacts using the StackReg plugin in Fiji/ImageJ with 'Rigid Body' or 'Translation' transformation. The movement-corrected max-z image sequence was used for subsequent analyses.

To generate a $\Delta F/F_0$ image, GCaMP6s images (typically of four time-points) before stimulation were averaged to generate a baseline F_0 image. GCaMP6s images (typically of three time-points) during peak response to a stimulation were max-intensity projected to generate an F_{max} image. The $\Delta F/F_0$ image was calculated as $(F_{max} - F_0)/F_0$ for each pixel. The only exception is the $\Delta F/F_0$ images for *Trh-Gal4s* (Figures 1A–1C). Because of the dense GCaMP6s-expressing arbors, movement correction was performed for each z-plane over time and a $\Delta F/F_0$ image was generated for each z-plane. The $\Delta F/F_0$ images for all z-plane were max-intensity projected to generate the final $\Delta F/F_0$ images shown in Figures 1A–1C. Image calculations were done in Matlab and $\Delta F/F_0$ images were displayed using Fiji/ImageJ.

To generate $\Delta F/F_0$ traces, regions of interest (ROIs) were manually drawn on GCaMP6s-expressing processes in Fiji/ImageJ, and the average fluorescence intensity of each ROI over time was measured using the Time Series Analyzer V3 plugin in Fiji/ImageJ. A large background ROI was drawn on areas without GCaMP6s expression, and the average fluorescence intensity of the background ROI for each time-point was subtracted from that of each ROI to generate a background-corrected ROI fluorescence intensity over time,

F(t). For each ROI F(t) trace, fluorescence intensity (typically of four time-points) before stimulation was averaged to generate a fluorescence baseline F_0, and $\Delta F/F_0$ was calculated as $(F(t) F_0)/F_0$ for each time-point (t). If multiple ROIs were drawn for a single cell/cell type, the $\Delta F/F_0$ traces for those ROIs were averaged to generate a mean $\Delta F/F_0$ trace for that cell/cell type. Max $\Delta F/F_0$ was the maximum $\Delta F/F_0$ value during and immediately after stimulation for a given $\Delta F/F_0$ done in Fiji/ImageJ. Intensity calculations were done in Matlab. Statistical tests were performed in Prism and reported in the figure legends.

Calcium imaging with optogenetics—The analyses of GCaMP6s imaging data for optogenetic experiments were performed in the same way as those described for the taste stimulation experiments except for the following: (1) Because only a single plane was imaged for the optogenetic experiments, max-intensity z-projection was not performed. (2) Typically, five time-points before stimulation were used to generate the F_0 images and F_0, and three to four time-points during peak response to stimulation were used to generate the F_{max} images. (3) The background fluorescence levels were very low in these images and often resulted in erroneously large pixel values when $\Delta F/F_0$ images were calculated. To minimize such errors, an intensity-based threshold was applied to the image sequence to exclude areas without GCaMP6s expression from calculations.

Temporal consumption assay—Feeding bouts of representative individuals (Figures 4A and 4C) were plotted in Matlab using the start and end times of each feeding bout. The total consumption time for each individual was the sum of the duration of each feeding bout. Statistical tests were performed in Prism and reported in the figure legends.

Quantification of Dilp2 immunostaining intensity—To quantify the immunostaining intensity of Dilp2 (Figure S2P), a region of interest (ROI) was manually drawn encircling the cytoplasm for each Dilp2+ cell, and the mean pixel intensity was calculated for each ROI using Fiji/ImageJ. Minimum and maximum pixel intensities were 0 and 4095, respectively. Statistical tests were performed in Prism and reported in the figure legends.

Crop contraction assay—To quantify crop contractions, a region of interest (ROI) was drawn encircling the crop, and the ROI frame-to-frame change of individual pixel intensity was calculated and summed per frame. This total change of pixel intensity per frame was then normalized to the pre-stimulation baseline (the 25th percentile of the 30 s pre-stimulation period) to generate a time-series fold change as shown in Figures 7B, 7D, 7F, and 7H. This quantification method accurately reflected the timing and amplitude of crop contractions as seen visually (Video S2). ROI drawing was done in Fiji/ImageJ and calculations were done in Matlab. Statistical tests were performed in Prism and reported in the figure legends.

Supplementary Material

Refer to Web version on PubMed Central for supplementary material.

ACKNOWLEDGMENTS

We thank Christoph Scheper and Michael D. Gordon for early work on the bitter-SELs and Christoph Scheper for identifying *VT46202-Gal4* and the *split-Gal4* line for bitter-SELs. Gabriella R. Sterne identified *split-Gal4* lines for sugar-SEL PNs and LNs. Brendan C. Mullaney generated *AKH-LexA*. Pierre Léopold provided Dilp2 antiserum. Two-photon imaging was conducted at the CRL Molecular Imaging Center, supported by NSF DBI-1041078 and the Helen Wills Neuroscience Institute. Julie H. Simpson, Hubert Amrein, David J. Anderson, Adam Claridge-Chang, Herman A. Dierick, Zhefeng Gong, Anthony Cammarato, Barry J. Dickson, Paul A. Garrity, Toshihiro Kitamoto, the Bloomington *Drosophila* Stock Center, and the Vienna *Drosophila* Resource Center provided fly stocks. This work was supported by a Jane Coffin Childs Fellowship to Z.Y. and an NIH grant R01GM128209 to K.S.

REFERENCES

Ahmad M, He L, and Perrimon N (2020). Regulation of insulin and adipokinetic hormone/glucagon production in flies. Wiley Interdiscip. Rev. Dev. Biol. 9, e360. [PubMed: 31379062]

Albin SD, Kaun KR, Knapp J-M, Chung P, Heberlein U, and Simpson JH (2015). A subset of serotonergic neurons evokes hunger in adult *Drosophila*. Curr. Biol. 25, 2435–2440. [PubMed: 26344091]

Alekseyenko OV, Lee C, and Kravitz EA (2010). Targeted manipulation of serotonergic neurotransmission affects the escalation of aggression in adult male *Drosophila* melanogaster. PLoS One 5, e10806. [PubMed: 20520823]

Augustine V, Gokce SK, Lee S, Wang B, Davidson TJ, Reimann F, Gribble F, Deisseroth K, Lois C, and Oka Y (2018). Hierarchical neural architecture underlying thirst regulation. Nature 555, 204–209. [PubMed: 29489747]

Betley JN, Xu S, Cao ZFH, Gong R, Magnus CJ, Yu Y, and Sternson SM (2015). Neurons for hunger and thirst transmit a negative-valence teaching signal. Nature 521, 180–185. [PubMed: 25915020]

Bidaye SS, Laturney M, Chang AK, Liu Y, Bockemühl T, Büschges A, and Scott K (2020). Two brain pathways initiate distinct forward walking programs in *Drosophila*. Neuron 108, 469–485.e8. [PubMed: 32822613]

Blenau W, Daniel S, Balfanz S, Thamm M, and Baumann A (2017). Dm5HT2B: pharmacological characterization of the fifth serotonin receptor subtype of *Drosophila* melanogaster. Front. Syst. Neurosci. 11, 28. [PubMed: 28553207]

Brand AH, and Perrimon N (1993). Targeted gene expression as a means of altering cell fates and generating dominant phenotypes. Development 118, 401–415. [PubMed: 8223268]

Calkins TL, DeLaat A, and Piermarini PM (2017). Physiological characterization and regulation of the contractile properties of the mosquito ventral diverticulum (crop). J. Insect Physiol. 103, 98–106. [PubMed: 29107658]

Chen C-L, Hermans L, Viswanathan MC, Fortun D, Aymanns F, Unser M, Cammarato A, Dickinson MH, and Ramdya P (2018). Imaging neural activity in the ventral nerve cord of behaving adult *Drosophila*. Nat. Commun. 9, 4390. [PubMed: 30348941]

Chen T-W, Wardill TJ, Sun Y, Pulver SR, Renninger SL, Baohan A, Schreiter ER, Kerr RA, Orger MB, Jayaraman V, et al. (2013). Ultrasensitive fluorescent proteins for imaging neuronal activity. Nature 499, 295–300. [PubMed: 23868258]

Chen Y, and Knight ZA (2016). Making sense of the sensory regulation of hunger neurons. BioEssays 38, 316–324. [PubMed: 26898524]

Chen Y, Lin Y-C, Kuo T-W, and Knight ZA (2015). Sensory detection of food rapidly modulates arcuate feeding circuits. Cell 160, 829–841. [PubMed: 25703096]

Cognigni P, Bailey AP, and Miguel-Aliaga I (2011). Enteric neurons and systemic signals couple nutritional and reproductive status with intestinal homeostasis. Cell Metab 13, 92–104. [PubMed: 21195352]

Colas JF, Launay JM, Kellermann O, Rosay P, and Maroteaux L (1995). *Drosophila* 5-HT2 serotonin receptor: coexpression with fushi-tarazu during segmentation. Proc. Natl. Acad. Sci. USA 92, 5441–5445. [PubMed: 7777527]

Donovan MH, and Tecott LH (2013). Serotonin and the regulation of mammalian energy balance. Front. Neurosci. 7, 36. [PubMed: 23543912]

Dus M, Lai JS-Y, Gunapala KM, Min S, Tayler TD, Hergarden AC, Geraud E, Joseph CM, and Suh GSB (2015). Nutrient sensor in the brain directs the action of the brain-gut axis in *Drosophila*. Neuron 87, 139–151. [PubMed: 26074004]

Fischer JA, Giniger E, Maniatis T, and Ptashne M (1988). GAL4 activates transcription in *Drosophila*. Nature 332, 853–856. [PubMed: 3128741]

Freeman EG, and Dahanukar A (2015). Molecular neurobiology of *Drosophila* taste. Curr. Opin. Neurobiol. 34, 140–148. [PubMed: 26102453]

French AS, Simcock KL, Rolke D, Gartside SE, Blenau W, and Wright GA (2014). The role of serotonin in feeding and gut contractions in the honeybee. J. Insect Physiol. 61, 8–15. [PubMed: 24374107]

Fujii S, Yavuz A, Slone J, Jagge C, Song X, and Amrein H (2015). *Drosophila* Sugar receptors in sweet taste perception, olfaction, and internal nutrient sensing. Curr. Biol. 25, 621–627. [PubMed: 25702577]

Fujita M, and Tanimura T (2011). *Drosophila* evaluates and learns the nutritional value of sugars. Curr. Biol. 21, 751–755. [PubMed: 21514154]

Géminard C, Rulifson EJ, and Léopold P (2009). Remote control of insulin secretion by fat cells in *Drosophila*. Cell Metab 10, 199–207. [PubMed: 19723496]

Gnerer JP, Venken KJT, and Dierick HA (2015). Gene-specific cell labeling using MiMIC transposons. Nucleic Acids Res 43, e56. [PubMed: 25712101]

Gordon MD, and Scott K (2009). Motor control in a *Drosophila* taste circuit. Neuron 61, 373–384. [PubMed: 19217375]

Hamada FN, Rosenzweig M, Kang K, Pulver SR, Ghezzi A, Jegla TJ, and Garrity PA (2008). An internal thermal sensor controlling temperature preference in *Drosophila*. Nature 454, 217–220. [PubMed: 18548007]

Hampel S, Chung P, McKellar CE, Hall D, Looger LL, and Simpson JH (2011). *Drosophila* brainbow: a recombinase-based fluorescence labeling technique to subdivide neural expression patterns. Nat. Methods 8, 253–259. [PubMed: 21297621]

Harris DT, Kallman BR, Mullaney BC, and Scott K (2015). Representations of taste modality in the *Drosophila* brain. Neuron 86, 1449–1460. [PubMed: 26051423]

Hernandez-Nunez L, Belina J, Klein M, Si G, Claus L, Carlson JR, and Samuel ADT (2015). Reverse-correlation analysis of navigation dynamics in *Drosophila* larva using optogenetics. Elife 4, 1–16.

Inagaki HK, Jung Y, Hoopfer ED, Wong AM, Mishra N, Lin JY, Tsien RY, and Anderson DJ (2014). Optogenetic control of *Drosophila* using a red-shifted channelrhodopsin reveals experience-dependent influences on courtship. Nat. Methods 11, 325–332. [PubMed: 24363022]

Ishita Y, Chihara T, and Okumura M (2020). Serotonergic modulation of feeding behavior in Caenorhabditis elegans and other related nematodes. Neurosci. Res. 154, 9–19. [PubMed: 31028772]

Jefferis GSXE, Potter CJ, Chan AM, Marin EC, Rohlfing T, Maurer CR, and Luo L (2007). Comprehensive maps of *Drosophila* higher olfactory centers: spatially segregated fruit and pheromone representation. Cell 128, 1187–1203. [PubMed: 17382886]

Joseph RM, Sun JS, Tam E, and Carlson JR (2017). A receptor and neuron that activate a circuit limiting sucrose consumption. Elife 6, 1–25.

Keene AC, and Masek P (2012). Optogenetic induction of aversive taste memory. Neuroscience 222, 173–180. [PubMed: 22820051]

Kim H, Kirkhart C, and Scott K (2017). Long-range projection neurons in the taste circuit of *Drosophila*. Elife 6, e23386. [PubMed: 28164781]

Kitamoto T (2001). Conditional modification of behavior in *Drosophila* by targeted expression of a temperature-sensitive shibire allele in defined neurons. J. Neurobiol. 47, 81–92. [PubMed: 11291099]

Klapoetke NC, Murata Y, Kim SS, Pulver SR, Birdsey-Benson A, Cho YK, Morimoto TK, Chuong AS, Carpenter EJ, Tian Z, et al. (2014). Independent optical excitation of distinct neural populations. Nat. Methods 11, 338–346. [PubMed: 24509633]

Lai S-L, and Lee T (2006). Genetic mosaic with dual binary transcriptional systems in *Drosophila*. Nat. Neurosci. 9, 703–709. [PubMed: 16582903]

Lam DD, Garfield AS, Marston OJ, Shaw J, and Heisler LK (2010). Brain serotonin system in the coordination of food intake and body weight. Pharmacol. Biochem. Behav. 97, 84–91. [PubMed: 20837046]

Lemaitre B, and Miguel-Aliaga I (2013). The digestive tract of *Drosophila* melanogaster. Annu. Rev. Genet. 47, 377–404. [PubMed: 24016187]

Leopold P, and Perrimon N (2007). *Drosophila* and the genetics of the internal milieu. Nature 450, 186–188. [PubMed: 17994083]

Li Q, and Gong Z (2015). Cold-sensing regulates *Drosophila* growth through insulin-producing cells. Nat. Commun. 6, 10083. [PubMed: 26648410]

Lin JY, Knutsen PM, Muller A, Kleinfeld D, and Tsien RY (2013). ReaChR: a red-shifted variant of channelrhodopsin enables deep transcranial optogenetic excitation. Nat. Neurosci. 16, 1499–1508. [PubMed: 23995068]

Liscia A, Solari P, Gibbons ST, Gelperin A, and Stoffolano JG (2012). Effect of serotonin and calcium on the supercontractile muscles of the adult blowfly crop. J. Insect Physiol. 58, 356–366. [PubMed: 22223038]

Luan H, Peabody NC, Vinson CR, and White BH (2006). Refined spatial manipulation of neuronal function by combinatorial restriction of transgene expression. Neuron 52, 425–436. [PubMed: 17088209]

Mandelblat-Cerf Y, Ramesh RN, Burgess CR, Patella P, Yang Z, Lowell BB, and Andermann ML (2015). Arcuate hypothalamic AgRP and putative POMC neurons show opposite changes in spiking across multiple timescales. Elife 4, 1–25.

Marella S, Fischler W, Kong P, Asgarian S, Rueckert E, and Scott K (2006). Imaging taste responses in the fly brain reveals a functional map of taste category and behavior. Neuron 49, 285–295. [PubMed: 16423701]

Marston OJ, Garfield AS, and Heisler LK (2011). Role of central serotonin and melanocortin systems in the control of energy balance. Eur. J. Pharmacol. 660, 70–79. [PubMed: 21216242]

Meda N, Frighetto G, Megighian A, and Zordan MA (2020). Searching for relief: *Drosophila melanogaster* navigation in a virtual bitter maze. Behav. Brain Res. 389, 112616. [PubMed: 32361039]

Meunier N, Marion-Poll F, Rospars J-P, and Tanimura T (2003). Peripheral coding of bitter taste in *Drosophila*. J. Neurobiol. 56, 139–152. [PubMed: 12838579]

Miguel-Aliaga I, Jasper H, and Lemaitre B (2018). Anatomy and physiology of the digestive tract of *Drosophila melanogaster*. Genetics 210, 357–396. [PubMed: 30287514]

Mohammad F, Stewart JC, Ott S, Chlebikova K, Chua JY, Koh T-W, Ho J, and Claridge-Chang A (2017). Optogenetic inhibition of behavior with anion channelrhodopsins. Nat. Methods 14, 271–274. [PubMed: 28114289]

Murthy M, and Turner G (2013). Whole-cell *in vivo* patch-clamp recordings in the *Drosophila* brain. Cold Spring Harb. Protoc. 2013, 140–148. [PubMed: 23378646]

Namiki S, Dickinson MH, Wong AM, Korff W, and Card GM (2018). The functional organization of descending sensory-motor pathways in *Drosophila*. Elife 7, 1–50.

Nässel DR, and Zandawala M (2020). Hormonal axes in *Drosophila*: regulation of hormone release and multiplicity of actions. Cell Tissue Res 382, 233–266. [PubMed: 32827072]

Nicolaï LJJ, Ramaekers A, Raemaekers T, Drozdzecki A, Mauss AS, Yan J, Landgraf M, Annaert W, and Hassan BA (2010). Genetically encoded dendritic marker sheds light on neuronal connectivity in *Drosophila*. Proc. Natl. Acad. Sci. USA 107, 20553–20558. [PubMed: 21059961]

Pfeiffer BD, Truman JW, and Rubin GM (2012). Using translational enhancers to increase transgene expression in *Drosophila*. Proc. Natl. Acad. Sci. USA 109, 6626–6631. [PubMed: 22493255]

Pfeiffer BD, Ngo TTB, Hibbard KL, Murphy C, Jenett A, Truman JW, and Rubin GM (2010). Refinement of tools for targeted gene expression in *Drosophila*. Genetics 186, 735–755. [PubMed: 20697123]

Pool A-H, Kvello P, Mann K, Cheung SK, Gordon MD, Wang L, and Scott K (2014). Four GABAergic interneurons impose feeding restraint in *Drosophila*. Neuron 83, 164–177. [PubMed: 24991960]

Pooryasin A, and Fiala A (2015). Identified serotonin-releasing neurons induce behavioral quiescence and suppress mating in *Drosophila*. J. Neurosci. 35, 12792–12812. [PubMed: 26377467]

Power ML, and Schulkin J (2008). Anticipatory physiological regulation in feeding biology: cephalic phase responses. Appetite 50, 194–206. [PubMed: 18045735]

Qian Y, Cao Y, Deng B, Yang G, Li J, Xu R, Zhang D, Huang J, and Rao Y (2017). Sleep homeostasis regulated by 5HT2B receptor in a small subset of neurons in the dorsal fan-shaped body of *Drosophila*. Elife 6, 1–27.

Sarnelli G, Annunziata G, Magno S, Oriolo C, Savastano S, and Colao A; Obesity Programs of Nutrition, Education, Research and Assessment (OPERA) Group (2019). Taste and the gastrointestinal tract: from physiology to potential therapeutic target for obesity. Int. J. Obes. Suppl. 9, 1–9. [PubMed: 31391920]

Schindelin J, Arganda-Carreras I, Frise E, Kaynig V, Longair M, Pietzsch T, Preibisch S, Rueden C, Saalfeld S, Schmid B, et al. (2012). Fiji: an open-source platform for biological-image analysis. Nat. Methods 9, 676–682. [PubMed: 22743772]

Schoofs A, Hückesfeld S, and Pankratz MJ (2018). Serotonergic network in the subesophageal zone modulates the motor pattern for food intake in *Drosophila*. J. Insect Physiol. 106, 36–46. [PubMed: 28735009]

Scott K, Brady R, Cravchik A, Morozov P, Rzhetsky A, Zuker C, and Axel R (2001). A chemosensory gene family encoding candidate gustatory and olfactory receptors in *Drosophila*. Cell 104, 661–673. [PubMed: 11257221]

Shearin HK, Dvarishkis AR, Kozeluh CD, and Stowers RS (2013). Expansion of the gateway multisite recombination cloning toolkit. PLOS One 8, e77724. [PubMed: 24204935]

Simpson JH (2016). Rationally subdividing the fly nervous system with versatile expression reagents. J. Neurogenet. 30, 185–194. [PubMed: 27846759]

Söderberg JAE, Carlsson MA, and Nässel DR (2012). Insulin-producing cells in the *Drosophila* brain also express satiety-inducing cholecystokinin-like peptide, drosulfakinin. Front. Endocrinol. (Lausanne) 3, 109. [PubMed: 22969751]

Solari P, Rivelli N, De Rose F, Picciau L, Murru L, Stoffolano JG, and Liscia A (2017). Opposite effects of 5-HT/AKH and octopamine on the crop contractions in adult *Drosophila melanogaster*: evidence of a double brain-gut serotonergic circuitry. PLoS One 12, e0174172. [PubMed: 28334024]

Sterne GR, Otsuna H, Dickson BJ, and Scott K (2021). Classification and genetic targeting of cell types in the primary taste and premotor center of the adult *Drosophila* brain. Elife 10, 805.

Stocker RF (1994). The organization of the chemosensory system in *Drosophila melanogaster*: a review. Cell Tissue Res 275, 3–26. [PubMed: 8118845]

Strother JA, Wu S-T, Wong AM, Nern A, Rogers EM, Le JQ, Rubin GM, and Reiser MB (2017). The emergence of directional selectivity in the visual motion pathway of *Drosophila*. Neuron 94, 168–182.e10. [PubMed: 28384470]

Tecott LH (2007). Serotonin and the orchestration of energy balance. Cell Metab 6, 352–361. [PubMed: 17983581]

Teff K (2000). Nutritional implications of the cephalic-phase reflexes: endocrine responses. Appetite 34, 206–213. [PubMed: 10744911]

Thistle R, Cameron P, Ghorayshi A, Dennison L, and Scott K (2012). Contact chemoreceptors mediate male-male repulsion and male-female attraction during *Drosophila* courtship. Cell 149, 1140–1151. [PubMed: 22632976]

Thorne N, Chromey C, Bray S, and Amrein H (2004). Taste perception and coding in *Drosophila*. Curr. Biol. 14, 1065–1079. [PubMed: 15202999]

Tierney AJ (2018). Invertebrate serotonin receptors: a molecular perspective on classification and pharmacology. J. Exp. Biol. 221, jeb184838. [PubMed: 30287590]

Tierney AJ (2020). Feeding, hunger, satiety and serotonin in invertebrates. Proc. Biol. Sci. 287, 20201386. [PubMed: 32781950]

Tirian L, and Dickson BJ (2017). The VT GAL4, LexA, and split-GAL4 driver line collections for targeted expression in the *Drosophila* nervous system. bioRxiv. bioRxiv. 10.1101/198648.

Vleugels R, Verlinden H, and Vanden Broeck J.. (2015). Serotonin, serotonin receptors and their actions in insects. NeuroTransmitter 2, e314.

Wang JW, Wong AM, Flores J, Vosshall LB, and Axel R (2003). Two-photon calcium imaging reveals an odor-evoked map of activity in the fly brain. Cell 112, 271–282. [PubMed: 12553914]

Wang P, Jia Y, Liu T, Jan Y-N, and Zhang W (2020). Visceral Mechanosensing neurons control *Drosophila* feeding by using piezo as a sensor. Neuron 108, 640–650.e4. [PubMed: 32910893]

Wang Z, Singhvi A, Kong P, and Scott K (2004). Taste representations in the *Drosophila* brain. Cell 117, 981–991. [PubMed: 15210117]

Wayland MT, Defaye A, Rocha J, Jayaram SA, Royet J, Miguel-Aliaga I, Leulier F, and Cognigni P (2014). Spotting the differences: probing host/ microbiota interactions with a dedicated software tool for the analysis of faecal outputs in *Drosophila*. J. Insect Physiol. 69, 126–135. [PubMed: 24907675]

Wyler SC, Lord CC, Lee S, Elmquist JK, and Liu C (2017). Serotonergic control of metabolic homeostasis. Front. Cell. Neurosci. 11, 277. [PubMed: 28979187]

Xie C, Wang X, Young RL, Horowitz M, Rayner CK, and Wu T (2018). Role of intestinal bitter sensing in enteroendocrine hormone secretion and metabolic control. Front. Endocrinol. (Lausanne) 9, 576. [PubMed: 30319553]

Yao Z, and Shafer OT (2014). The *Drosophila* circadian clock is a variably coupled network of multiple peptidergic units. Science 343, 1516–1520. [PubMed: 24675961]

Yarmolinsky DA, Zuker CS, and Ryba NJP (2009). Common sense about taste: from mammals to insects. Cell 139, 234–244. [PubMed: 19837029]

Zafra MA, Molina F, and Puerto A (2006). The neural/cephalic phase reflexes in the physiology of nutrition. Neurosci. Biobehav. Rev. 30, 1032–1044. [PubMed: 16678262]

Zhang YQ, Rodesch CK, and Broadie K (2002). Living synaptic vesicle marker: synaptotagmin-GFP. Genesis 34, 142–145. [PubMed: 12324970]

Zimmerman CA, Lin Y-C, Leib DE, Guo L, Huey EL, Daly GE, Chen Y, and Knight ZA (2016). Thirst neurons anticipate the homeostatic consequences of eating and drinking. Nature 243, 297–307.

Highlights

- Sugar and bitter tastes activate distinct populations of 5-HT neurons in Drosophila
- Sugar-responsive 5-HT neurons promote insulin release and prevent overconsumption
- Bitter-responsive 5-HT neurons activate enteric neurons to promote gastric motility
- 5-HT neurons translate gustatory detection into anticipatory physiological changes

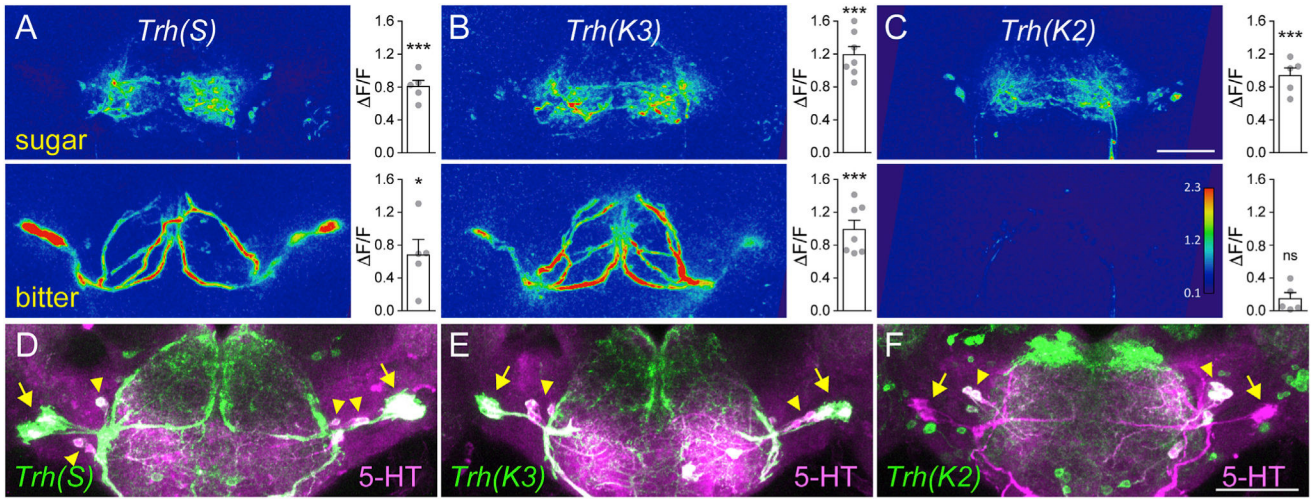

Figure 1. Sugar and bitter activate different SEZ 5-HT neurons

(A–C) Left: representative $\Delta F/F_0$ images of GCaMP6s imaging showing dorsal SEZ 5-HT neurons responding to sugar (upper panels) and bitter (lower panels) proboscis taste detection. For all taste imaging experiments, sugar stimulation was 1-M sucrose, and bitter stimulation was 100-mM caffeine, 10-mM denatonium, and 20% polyethylene glycol (PEG). GcaMP6s was expressed using three *Trh-Gal4* (*Trh: tryptophan hydroxylase*) lines (D–F). Right: maximum $\Delta F/F_0$ changes for individual flies (dots) and bar plot overlay, mean ± SEM. n = 5–7 flies/genotype; paired t test to pre-stimulation baseline, *p < 0.05, ***p < 0.001, ns, not significant. Scale bars, 50 μm.

(D–F) *Trh-Gal4* lines were characterized using *UAS-CD8-GFP* expression (green). Antibody staining against 5-HT is shown in magenta. Arrowheads denote three 5-HT neural pairs with smaller somas and arrows denote two 5-HT neural pairs with larger somas. Scale bars, 50 μm.

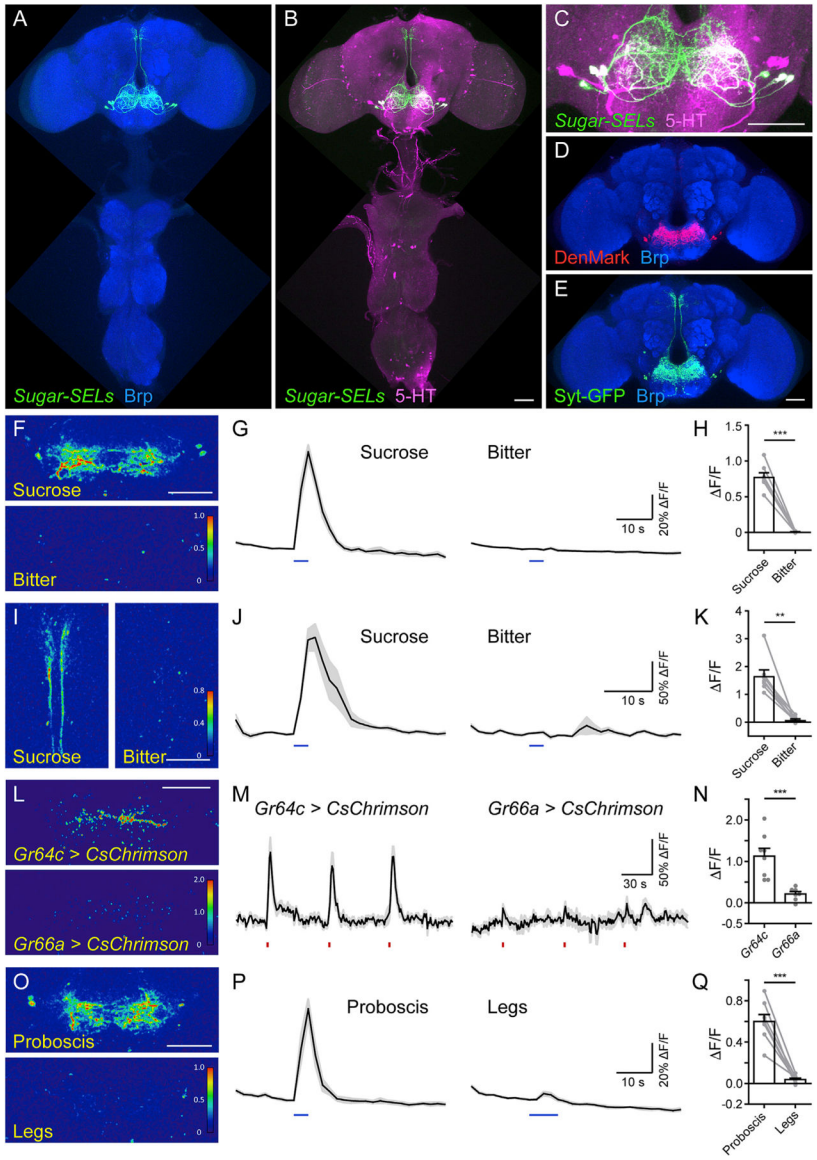

Figure 2. Sugar-SELs respond to proboscis sugar detection

(A–C) Sugar-SELs are labeled by the genetic intersection between *Trh-Gal4(K2)* and *Dfd-LexA* (green). Anti-Brp (A) labels brain and VNC neuropil (blue). Anti-5-HT (B and C) shows 5-HT neurons (magenta). (C) is a magnified image of (B). Scale bars, 50 μm.

(D and E) Dendrites (D, DenMark, red) and axons (E, Syt-GFP, green) of sugar-SELs (*Trh(K2)*∩*Dfd*). Anti-Brp labels neuropil (blue). Scale bars, 50 μm.

(F–H) Sugar-SEL (*Trh(K2)*∩*Dfd*) arbors in SEZ respond to proboscis sucrose but not bitter detection.

(I–K) Sugar-SEL (*Trh(K2)*∩*Dfd*) projections along the median bundle respond to proboscis sucrose but not bitter detection.

(L–N) Sugar-SEL PNs (*SEZ-205*) respond to CsChrimson-mediated optogenetic excitation of sugar (*Gr64c*$^{+}$) but not bitter (*Gr66a*$^{+}$) GRNs.

(O–Q) Sugar-SELs (*Trh(K2)*∩*Dfd*) respond to sucrose detection on the proboscis but not on the legs.

Images in (F), (I), (L), and (O) are representative $\Delta F/F_0$ images of GcaMP6s responses. Scale bars, 50 μm. Plots in (G), (J), (M), and (P) show mean $\Delta F/F_0$ traces (black lines) ± SEM (gray shading). Blue bars in (G) and (J) indicate sucrose (left) or bitter (right) stimulation. Red bars in (M) indicate red light stimulations. Blue bars in (P) indicate sucrose stimulation on the proboscis (left) or legs (right). (H) (K), (N), and (Q) are scatter plots of maximum $\Delta F/F_0$ changes, with bar plot overlay, mean ± SEM. (H), (K), and (Q): n = 8 flies; paired t test, **p < 0.01, ***p < 0.001. (N) n = 8 *Gr64c* flies, n = 7 *Gr66a* flies; Mann-Whitney test, ***p < 0.001. See Video S1 for sugar-SEL anatomy. See Figure S1 for additional analysis of sugar-SEL subtypes.

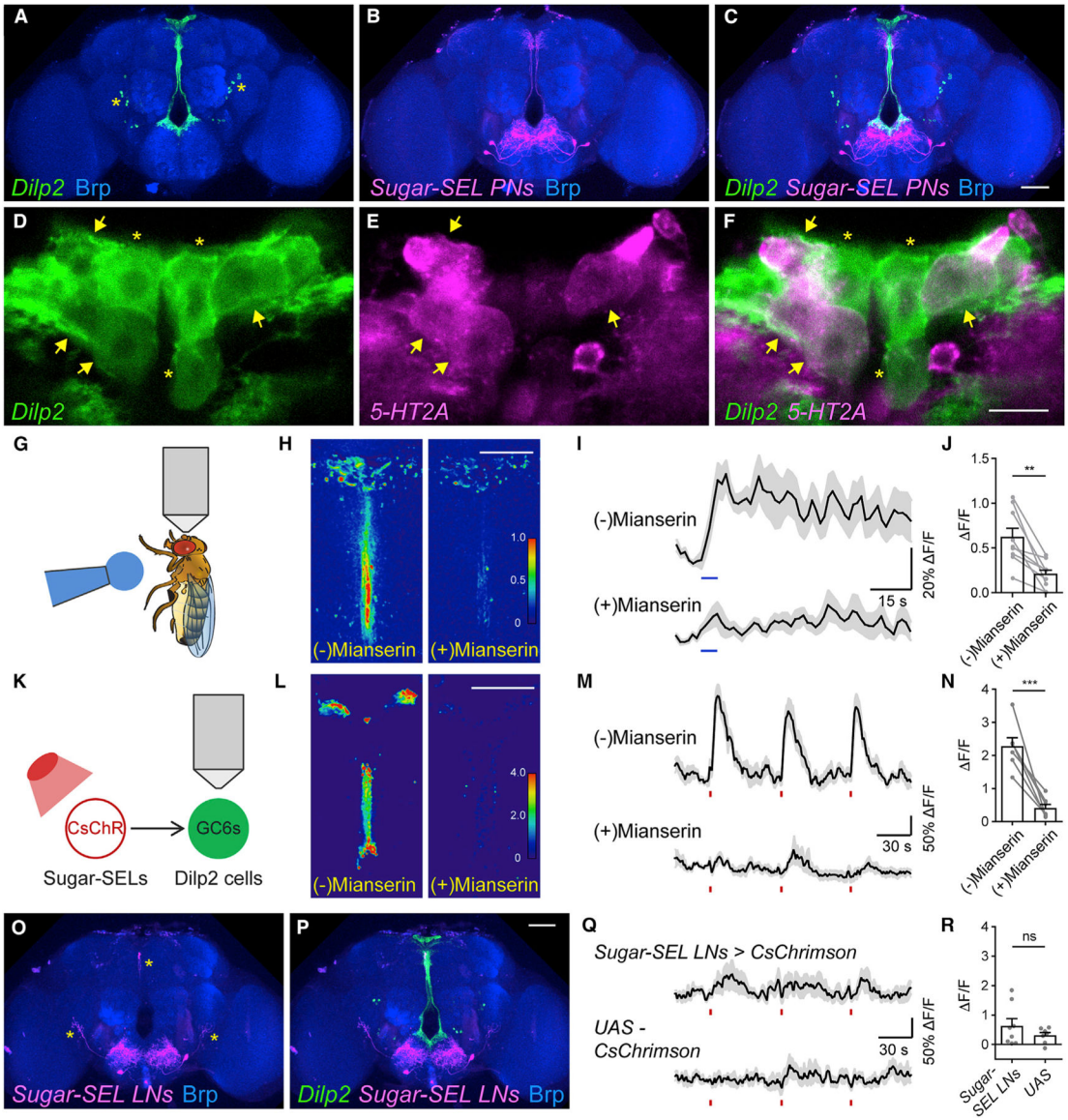

Figure 3. Sugar-SEL PNs excite insulin-producing cells

(A–C) Proximity of Dilp2 IPCs (*Dilp2-LexA>LexAop-CD8-GFP*, green) and sugar-SEL PNs (*SEZ-205>UAS-CD8-RFP*, magenta). Anti-Brp labels neuropil (blue). Yellow asterisks (A) mark non-specific cells labeled by *Dilp2-LexA*. Scale bars, 50 μm.

(D–F) A Dilp2 subset expresses 5-HT2A. Dilp2 cells are labeled by *Dilp2-LexA>LexAop-CD8-GFP* (green). 5-HT2A expressing cells are labeled by *5-HT2A [MI00459]-Gal4>UAS-CD8-RFP* (magenta). Yellow arrows mark Dilp2 cells that express 5-HT2A; yellow asterisks mark Dilp2 cells that do not express 5-HT2A. Scale bars, 10 μm.

(G–J) Dilp2 cells respond to proboscis sucrose detection. (G) Experiment schematic. (H) Representative GcaMP6s $\Delta F/F_0$ images of Dilp2 responses in the absence (left) or presence (right) of 100 μm mianserin, a 5-HT2 receptor antagonist. Scale bars, 50 μm. (I) Mean $\Delta F/F_0$ traces (black lines) ± SEM (gray shading). Blue bars indicate proboscis sucrose

stimulation. (J) Scatter plots of maximum $\triangle F/F_0$ changes, with bar plot overlay, mean ± SEM. n = 9 flies; paired t test, *p < 0.01.

(K–N) Dilp2 cells respond to optogenetic excitation of sugar-SEL PNs (*SEZ-205*). (K) Experiment schematic. CsChrimson (CsChR) was expressed in sugar-SEL PNs while GCaMP6s (GC6s) was expressed in Dilp2 cells. (L) Representative GCaMP6s $\triangle F/F_0$ images of Dilp2 responses in the absence (left) or presence (right) of 100 μm mianserin. Scale bars, 50 μm. (M) Mean $\triangle F/F_0$ traces (black lines) ± SEM (gray shading). Red bars indicate red light stimulations. (N) Scatter plots of maximum $\triangle F/F_0$, with bar plot overlay, mean ± SEM. n = 7 flies; paired t test, ***p < 0.001.

(O and P) Co-labeling of sugar-SEL LNs (*SEZ-569>UAS-CD8-RFP*, magenta) and Dilp2 IPCs (*Dilp2-LexA>LexAop-CD8-GFP*, green). Anti-Brp labels neuropil (blue). Yellow asterisks in (O) mark other cells labeled by *SEZ-569*. Scale bars, 50 μm.

(Q and R) Dilp2 cells do not respond to optogenetic excitation of sugar-SEL LNs (*SEZ-569*). (Q) Mean $\triangle F/F_0$ traces (black lines) ± SEM (gray shading) of Dilp2 cells in experimental (*Sugar-SEL LNs>CsChrimson*) and control flies (*UAS-CsChrimson*). Red bars indicate red light stimulations. (R) Scatter plots of maximum $\triangle F/F_0$ changes, with bar plot overlay, mean ± SEM. n = 8 sugar-SEL LNs flies, n = 7 *UAS* flies; Mann-Whitney test, ns, not significant. See Figure S2 for additional characterization of Dilp2 cells.

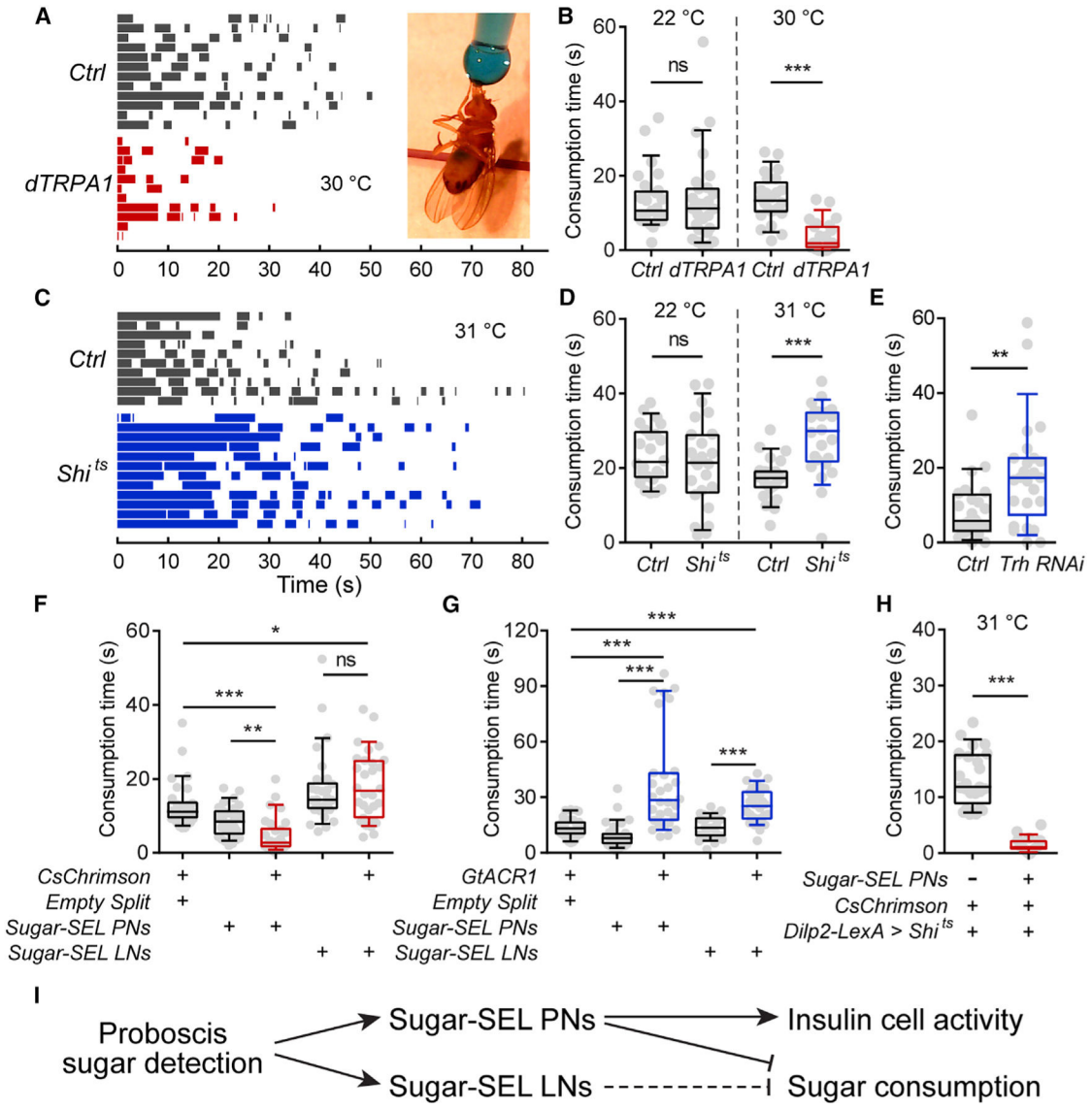

Figure 4. Sugar-SELs limit sugar intake

(A and B) Representative feeding bouts (A) and total consumption time (B) of control flies (*Ctrl*) and flies with *dTRPA1* in sugar-SELs (*dTRPA1, Trh(K2)∩Dfd*) at the indicated temperatures. dTRPA1 is active at 30°C and not active at 22°C. Inset (A) shows a fly drinking sucrose (blue). n = 24–27 flies/genotype; Mann-Whitney test, ***p < 0.001; ns, not significant.

(C and D) Representative feeding bouts (C) and total consumption time (D) of control flies (*Ctrl*) and flies with *Shits* in sugar-SELs (*Shits, Trh(K2)∩Dfd*) at the indicated temperatures. *Shi^{ts}* is dominant-negative at 31°C but not at 22°C. n = 23–24 flies/genotype; Mann-Whitney test, ***p < 0.001; ns, not significant.

(E) Total consumption time of control flies (*Ctrl*) and flies with *Trh* RNAi in sugar-SELs (*Trh RNAi, Trh(K2)∩Dfd*). n = 24–25 flies/genotype; Mann-Whitney test, **p < 0.01.

(F) Consumption time of control flies and flies with sugar-SEL PNs (*SEZ-205*) or sugar-SEL LNs (*SEZ-569*) excited using CsChrimson. n = 30 flies/genotype; Kruskal-Wallis

ANOVA followed by Dunn's multiple comparisons tests, *p < 0.05; **p < 0.01; ***p < 0.001; ns, not significant.

(G) Consumption time of control flies and flies with sugar-SEL PNs (*SEZ-205*) or sugar-SEL LNs (*SEZ-569*) silenced using GtACR1. n = 30 flies/genotype; Kruskal-Wallis ANOVA followed by Dunn's multiple comparisons tests, ***p < 0.001.

(H) Consumption time of control flies (black) and flies with sugar-SEL PNs (*SEZ-205*) excited using CsChrimson (red) upon silencing of Dilp2 cells with Shi^{ts}. n = 24 flies/genotype; Mann-Whitney test, ***p < 0.001.

(I) Model of sugar-SEL PN and LN function. Horizontal bars in (A) and (C) show feeding bouts of individual flies (one line per fly). 1-M sucrose was used for all panels. For box plots, whiskers = 10^{th}–90^{th} percentile, box = 25^{th}–75^{th} percentile, and line in box = median. Dots indicate individual data.

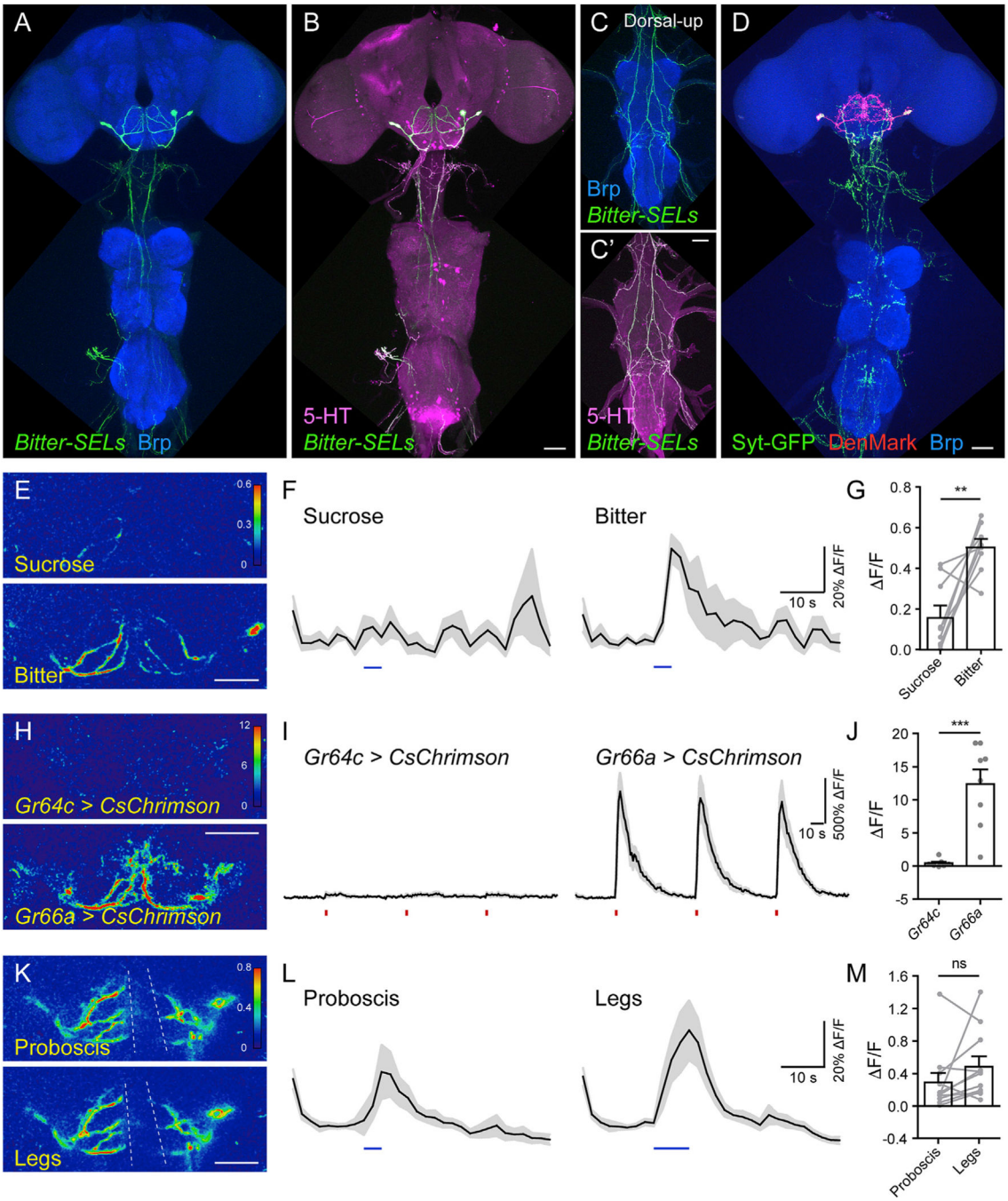

Figure 5. Bitter-SELs respond to bitter taste detection

(A–C) Bitter-SELs are labeled by the genetic intersection between *VT46202-Gal4* and *Dfd-LexA* (green). (C) and (C0) show bitter-SEL processes in the VNC in a dorsal-up view. Anti-Brp (A and C) labels neuropil (blue). Anti-5-HT (B and C0) shows 5-HT neurons and processes (magenta). Scale bars, 50 μm.

(D) Dendrites (DenMark, red) and axons (Syt-GFP, green) of bitter-SELs (*VT46202*∩*Dfd*). Anti-Brp labels neuropil (blue). Scale bars, 50 μm.

(E–G) Bitter-SELs (*DN052*) respond to proboscis bitter taste detection.

(H–J) Bitter-SELs (*VT46202*) respond to CsChrimson-mediated optogenetic excitation of bitter (*Gr66a*$^{+}$) but not sugar (*Gr64c*$^{+}$) GRNs.
(K–M) Bitter-SELs (*VT46202*) respond to bitter detection on the proboscis and legs.
Images in (E), (H), and (K) are representative $\Delta F/F_0$ images of GCaMP6s responses. Scale bars, 50 μm. White dotted lines in (K) indicate the esophagus. Plots in (F), (I), and (L) show mean $\Delta F/F_0$ traces (black lines) ± SEM (gray shading). Blue bars (F) indicate proboscis sucrose (left) or bitter (right) stimulation. Red bars (I) indicate red light stimulations. Blue bars (L) indicate bitter stimulation on the proboscis (left) or legs (right). (G), (J), and (M) are scatter plots of maximum $\Delta F/F_0$ changes, with bar plot overlay, mean ± SEM. (G): n = 9 flies; paired t test, **p < 0.01. (J): n = 7 *Gr64c* flies, n = 8 *Gr66a* flies; Mann-Whitney test, ***p < 0.001. (M): n = 11 flies; paired t test, ns, not significant. See Video S1 for bitter-SEL anatomy. See Figure S3 for additional characterization of bitter-SELs.

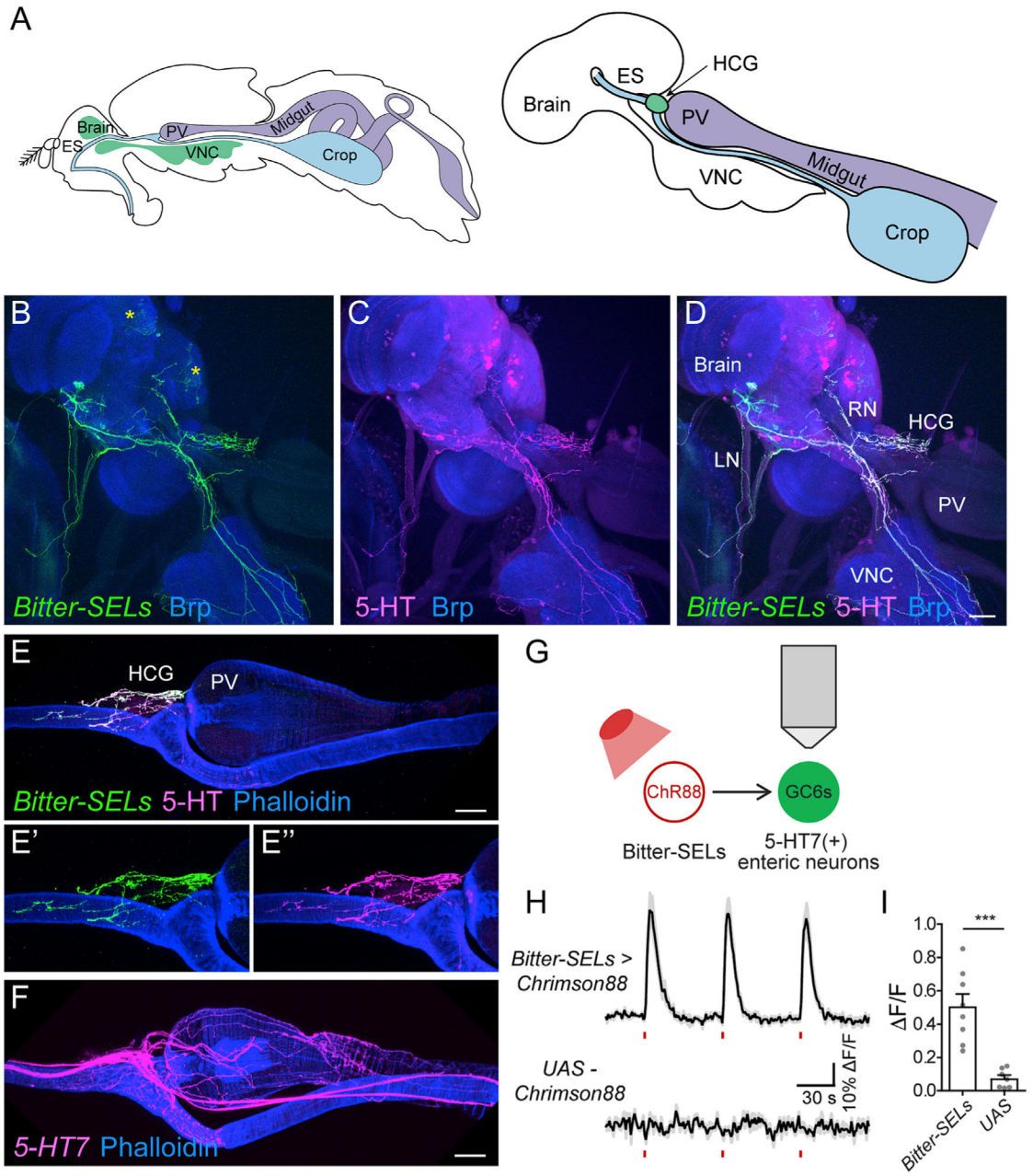

Figure 6. Bitter-SELs activate 5-HT7 enteric neurons

(A) Left: central nervous system (green), esophagus and crop (blue), and the rest of the digestive tract (purple). Right: the relative position of the central nervous system and digestive tract as shown in (B–D). VNC, ventral nerve cord; ES, esophagus; PV, proventriculus; HCG, hypocerebral ganglion.

(B–D) Bitter-SEL processes are labeled by *DN052>UAS-CD8-GFP* (green). Yellow asterisks (B) mark non-specific cells labeled by *DN052*. Anti-5-HT shows 5-HT neurons and processes (magenta). Anti-Brp labels neuropil (blue). LN, labial nerves; RN, recurrent nerve. Scale bars, 50 μm.

(E–E") A close-up view of bitter-SEL processes (*DN052*, green) in the hypocerebral ganglion (HCG) in a different fly. Anti-5-HT (magenta); Phalloidin stains the digestive tract (blue). Scale bars, 50 μm.

(F) 5-HT7-expressing enteric neurons are labeled by *5-HT7[MI00215]-Gal4>UAS-CD8-RFP* (magenta). Phalloidin stains the digestive tract (blue). Scale bars, 50 μm.

(G–I) Optogenetic excitation of bitter-SELs (*DN052*) activates 5-HT7(+) enteric neurons. (G) Chrimson88 (ChR88) was expressed in bitter-SELs while GCaMP6s (GC6s) was expressed in 5-HT7(+) enteric neurons. (H) Mean $\Delta F/F_0$ traces (black lines) ± SEM (gray shading) of 5-HT7(+) enteric neurons in experimental flies (*Bitter-SELs>UAS-Chrimson88*) and control flies (*UAS-Chrimson88*). Red bars indicate red light stimulations. (I) Scatter plots of maximum $\Delta F/F_0$ changes, with bar plot overlay, mean ± SEM. n = 8 bitter-SELs flies, n = 7 *UAS* flies; Mann-Whitney test, ***p < 0.001. See Figure S4 for additional analysis of bitter-SELs, AKH cells, and 5-HT receptor expression in HCG.

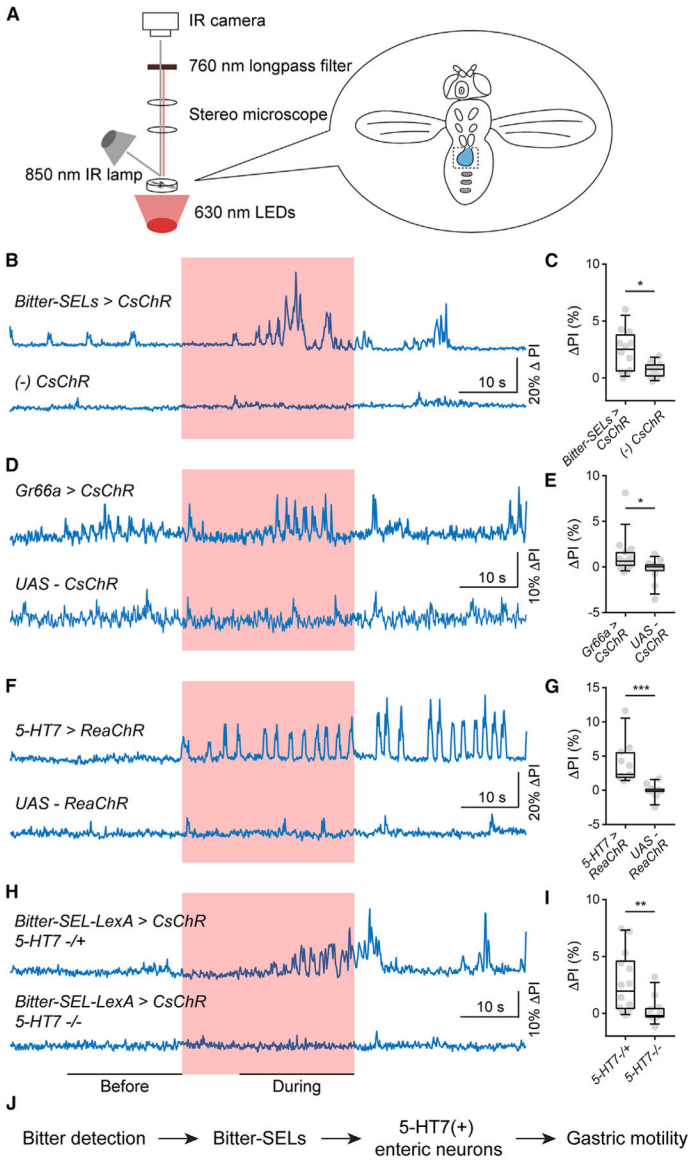

Figure 7. Optogenetic excitation of bitter-SELs promote crop contractions through 5-HT7

(A) Assay to video-record crop contractions in live flies in conjunction with simultaneous optogenetic stimulation.

(B–I) Representative traces (left) and quantification (right) of crop contractions in flies of the indicated genotypes. *Bitter-SELs*, *VT46202∩Dfd*; *Gr66a*, *Gr66a-Gal4*; *5-HT7*, 5-HT7[MI00215]-*Gal4*; *bitter-SEL-LexA*, *R24F06-LexA*. The red-shaded area in (B), (D), (F), and (H) indicates 630-nm light stimulation.

(C), (E), (G), and (I) quantify the net increase of crop contractions during optogenetic stimulation (during and before, time windows as illustrated in H) for the indicated genotypes. DPI, normalized fold change of pixel intensity. See STAR Methods for details. n = 11–15 flies/genotype; Mann-Whitney test, *p < 0.05, **p < 0.01, ***p < 0.001.

(J) Summary model for bitter-SEL function.

For box plots, whiskers = 1^{0t}h–9^{0t}h percentile, box = 2^{5t}h–7^{5t}h percentile, and line in box = median. See Video S2 for an example of crop contractions induced by bitter-SEL excitation. See Figure S3 for the expression pattern of *bitter-SEL-LexA* (*R24F06-LexA*).

KEY RESOURCES TABLE

REAGENT or RESOURCE	SOURCE	IDENTIFIER
Antibodies		
Chicken anti-GFP, polyclonal (1:500 dilution)	Thermo Fisher Scientific	Cat # A10262; RRID: AB_2534023
Rabbit anti-DsRed, polyclonal (1:500 dilution)	Takara Bio	Cat # 632496; RRID: AB_10013483
Rabbit anti-5-HT (serotonin), polyclonal (1:500 dilution)	MilliporeSigma	Cat # S5545; RRID: AB_477522
Mouse anti-Brp (nc82), monoclonal (1:500 dilution)	Developmental Studies Hybridoma Bank	RRID: AB_2314866
Rat anti-Dilp2, polyclonal (1:100 dilution)	(Géminard et al., 2009)	N/A
Goat anti-Chicken, Alexa 488 (1:1000 dilution)	Thermo Fisher Scientific	Cat # A-11039; RRID: AB_2534096
Goat anti-Rabbit, Alexa 568 (1:1000 dilution)	Thermo Fisher Scientific	Cat # A-11036; RRID: AB_10563566
Goat anti-Mouse, Alexa 647 (1:1000 dilution)	Thermo Fisher Scientific	Cat # A-21236; RRID: AB_2535805
Goat anti-Rat, Alexa 488 (1:1000 dilution)	Thermo Fisher Scientific	Cat # A-11006; RRID: AB_2534074
Phalloidin Alexa 633 (1:500 dilution of 5 unit/μL)	Thermo Fisher Scientific	Cat # A22284
Chemicals, peptides, and recombinant proteins		
Caffeine (CAS # 58-08-2)	MilliporeSigma	Cat # C0750
Denatonium benzoate (CAS # 3734-33-6)	MilliporeSigma	Cat # D5765
Poly(ethylene glycol) (PEG) (CAS # 25322-68-3)	MilliporeSigma	Cat # P4338
All trans-Retinal (CAS # 116-31-4)	MilliporeSigma	Cat # R2500
Bromophenol Blue sodium salt (CAS # 34725-61-6)	MilliporeSigma	Cat # B8026
Mianserin hydrochloride (CAS # 21535-47-7)	Tocris Bioscience	Cat # 0997
Experimental models: Organisms/strains		
Drosophila melanogaster: w[1118];; 10XUAS-IVS-mCD8::GFP(su(Hw)attP1)	Bloomington Drosophila Stock Center	RRID: BDSC_32187
Drosophila melanogaster: w[1118];; 13XLexAop2-IVS-myr::GFP(su(Hw)attP1)	Bloomington Drosophila Stock Center	RRID: BDSC_32212
Drosophila melanogaster: y[1] w[*]; UAS-mCD8::GFP.L(LL5)	Bloomington Drosophila Stock Center	RRID: BDSC_5137
Drosophila melanogaster: y[1] w[*]; Sp/CyO; Trh-Gal4.S(attP2)	Bloomington Drosophila Stock Center	RRID: BDSC_52249
Drosophila melanogaster: w[1118]; Trh-Gal4.long(2);	Bloomington Drosophila Stock Center	RRID: BDSC_38388
Drosophila melanogaster: w[1118];; Trh-Gal4.long(3)	Bloomington Drosophila Stock Center	RRID: BDSC_38389
Drosophila melanogaster: UAS-CD8-tdTomato;;	(Thistle et al., 2012)	N/A
Drosophila melanogaster: w[1118]; 20XUAS-IVS-GCaMP6s(attP40);	Bloomington Drosophila Stock Center	RRID: BDSC_42746
Drosophila melanogaster: w[1118];; 20XUAS-IVS-GCaMP6s(VK00005)	Bloomington Drosophila Stock Center	RRID: BDSC_42749
Drosophila melanogaster: w[1118];; 13XLexAop2-IVS-GCaMP6s(su(Hw)attP1)	Bloomington Drosophila Stock Center	RRID: BDSC_44273
Drosophila melanogaster: w,tub-FRT-Gal80-FRT(8-3);;	(Gordon and Scott, 2009)	N/A

REAGENT or RESOURCE	SOURCE	IDENTIFIER
Drosophila melanogaster: w[1118]; 8XLexAop2-FLPL(attP40);	Bloomington Drosophila Stock Center	RRID: BDSC_55820
Drosophila melanogaster: w[1118];; 8XLexAop2-FLPL(attP2)	Bloomington Drosophila Stock Center	RRID: BDSC_55819
Drosophila melanogaster:;; Dfd-LexA/TM3,Sb	(Simpson, 2016)	N/A
Drosophila melanogaster: w[1118]; UAS-DenMark(2),UAS-syt.eGFP(2); In(3L)D, mirr D[1]/TM6C, Sb[1]	Bloomington Drosophila Stock Center	RRID: BDSC_33064
Drosophila melanogaster: w[1118]; L[1]/CyO; UAS-DenMark(3),UAS-syt.eGFP(3)	Bloomington Drosophila Stock Center	RRID: BDSC_33065
Drosophila melanogaster:; R20G07-p65.AD (attP40)/CyO; VT043685-Gal4.DBD(attP2) (SEZ-205)	(Sterne et al., 2021) and Janelia Research Campus	JRC_SS35814
Drosophila melanogaster:; R19C05-p65.AD (attP40)/CyO; VT013872-Gal4.DBD(attP2) (SEZ-569)	(Sterne et al., 2021) and Janelia Research Campus	JRC_SS47232
Drosophila melanogaster: w[1118]; R24F06-p65.AD(attP40)/ CyO; R45E06-Gal4.DBD (attP2)/TM6B, Tb (DN052)	Bloomington Drosophila Stock Center	RRID: BDSC_75837
Drosophila melanogaster: w[1118]; p65.AD.Uw (attP40); Gal4.DBD.Uw(attP2) (Empty Split)	Bloomington Drosophila Stock Center	RRID: BDSC_79603
Drosophila melanogaster: w[1118]; R24F06-lexA(attP40); (bitter-SEL LexA)	Bloomington Drosophila Stock Center	RRID: BDSC_52695
Drosophila melanogaster:;; Gr64c-LexA(knockin)	(Fujii et al., 2015)	N/A
Drosophila melanogaster: Gr66a-LexA;;	(Thistle et al., 2012)	N/A
Drosophila melanogaster:; Gr66a-Gal4/CyO; TM2/TM6B	(Scott et al., 2001)	N/A
Drosophila melanogaster: w[1118], 13XLexAop2-IVS-CsChrimson.mVenus(attP18);;	Bloomington Drosophila Stock Center	RRID: BDSC_55137
Drosophila melanogaster: w[1118],20XUAS-IVS-CsChrimson.mVenus(attP18);;	Bloomington Drosophila Stock Center	RRID: BDSC_55134
Drosophila melanogaster: 10XUAS-Syn21-Chrimson88-tdT3.1(attP18),LexAop2-Syn21-opGCaMP6s(su(Hw)attP8);;	(Strother et al., 2017)	N/A
Drosophila melanogaster: w[*]; UAS-ReaChR(su(Hw)attP5)/ CyO;	Bloomington Drosophila Stock Center	RRID: BDSC_53748
Drosophila melanogaster:;; 20XUAS-IVS-GtACR1-EYFP(attP2)	(Mohammad et al., 2017)	N/A
Drosophila melanogaster: y[1] w[*], 10XUAS-IVS-mCD8::RFP(attP18), 13XLexAop2-mCD8::GFP(su(Hw)attP8);;	Bloomington Drosophila Stock Center	RRID: BDSC_32229
Drosophila melanogaster:; Dilp2-LexA; Sb/TM6B,Tb	(Li and Gong, 2015)	N/A
Drosophila melanogaster: w[*]; Dilp2-Gal4/CyO;	Bloomington Drosophila Stock Center	RRID: BDSC_37516
Drosophila melanogaster: w[1118]; AKH-LexA(attP40);	Brendan C. Mullaney, This paper	N/A
Drosophila melanogaster: w[1118];; Dh44-GAL4.TH(2M)	Bloomington Drosophila Stock Center	RRID: BDSC_51987
Drosophila melanogaster:; 5-HT1A-Gal4;	(Gnerer et al., 2015)	N/A
Drosophila melanogaster:; 5-HT1B-Gal4;	(Gnerer et al., 2015)	N/A
Drosophila melanogaster:;; 5-HT2A-Gal4	(Gnerer et al., 2015)	N/A
Drosophila melanogaster:;; 5-HT2B-Gal4	(Gnerer et al., 2015)	N/A
Drosophila melanogaster:;; 5-HT7-Gal4	(Gnerer et al., 2015)	N/A
Drosophila melanogaster:;; 5-HT7	Bloomington Drosophila Stock Center	RRID: BDSC_86279
Drosophila melanogaster:;; 5-HT7-T2A-LexA	Bloomington Drosophila Stock Center	RRID: BDSC_84354
Drosophila melanogaster:; UAS-dTRPA1/CyO;	(Hamada et al., 2008)	N/A

REAGENT or RESOURCE	SOURCE	IDENTIFIER
Drosophila melanogaster:; UAS-Shi^{ts};	(Kitamoto, 2001)	N/A
Drosophila melanogaster:;; LexAop2-Syn21-Shi^{ts}-p10(VK00005)	(Pfeiffer et al., 2012)	N/A
Drosophila melanogaster: w[1118],UAS-Dcr-2.D(1); Pin[1]/CyO;	Bloomington Drosophila Stock Center	RRID: BDSC_24644
Drosophila melanogaster:; UAS-Trh-RNAi;	Vienna Drosophila Resource Center	105414
Drosophila melanogaster: y[1] sc[*] v[1] sev[21];; UAS-5-HT2A-RNAi(VALIUM20)(attP2)	Bloomington Drosophila Stock Center	RRID: BDSC_56870
Drosophila melanogaster: y[1] sc[*] v[1] sev[21];; UAS-mCherry-RNAi(VALIUM20)(attP2)	Bloomington Drosophila Stock Center	RRID: BDSC_35785
Drosophila melanogaster:;; VT46202-Gal4	(Tirian and Dickson, 2017)	N/A
Drosophila melanogaster: Act88F:Rpr(attP18);;	(Chen et al., 2018)	N/A
Drosophila melanogaster: y[1] w[67c23] Crey(1b); sna/CyO; Dr[1]/TM3,Sb[1]	Bloomington Drosophila Stock Center	RRID: BDSC_34516
Drosophila melanogaster: w[1118]; UAS-Brainbow(attP40);	Bloomington Drosophila Stock Center	RRID: BDSC_34514
Software and algorithms		
Matlab	MathWorks	https://www.mathworks.com/products/matlab.html
Prism	GraphPad	https://www.graphpad.com/scientific-software/prism/
Fiji/ImageJ	(Schindelin et al., 2012)	https://imagej.net/Fiji
Computational Morphometry Toolkit (CMTK)	NeuroImaging Tools & Resources Collaboratory	https://www.nitrc.org/projects/cmtk/
FluoRender	University of Utah	https://www.sci.utah.edu/software/fluorender.html
The Ultimate Reader of Dung	(Wayland et al., 2014)	https://sourceforge.net/projects/the-ultimate-reader-of-dung/
Custom Matlab codes for analyzing calcium imaging data and crop contractions	This paper	https://doi.org/10.5281/zenodo.5774242